МІНІСТЕРСТВО ОСВІТИ І НАУКИ УКРАЇНИ
НАЦІОНАЛЬНИЙ АВІАЦІЙНИЙ УНІВЕРСИТЕТ
КАФЕДРА КОНСТРУКЦІЇ ЛІТАЛЬНИХ АПАРАТІВ

ДОПУСТИТИ ДО ЗАХИСТУ
Завідувач кафедри д.т.н, проф.
_____Сергій ІГНАТОВИЧ
«___» _____ 2022

ДИПЛОМНА РОБОТА
ВИПУСКНИКА ОСВІТНЬОГО СТУПЕНЯ МАГІСТРА
ЗІ СПЕЦІАЛЬНОСТІ
«АВІАЦІЙНА ТА РАКЕТНО-КОСМІЧНА ТЕХНІКА»

Тема: «Дослідження зображень інфрачервоного неруйнівного контролю полімерних композитів, армованих скловолокном»

Виконавець: _____ **Цзюньцзян ЧЖОУ**

Керівник: д.т.н., професор _____ **Михайло КАРУСКЕВИЧ**

Охорона праці: к.т.н., доцент _____ **Катерина КАЖАН**

Охорона навколишнього середовища:
к.т.н., доцент _____ **Леся ПАВЛЮХ**

Нормоконтролер: к.т.н., доцент _____ **Володимир КРАСНОПОЛЬСЬКИЙ**

Київ 2022

MINISTRY OF EDUCATION AND SCIENCE OF UKRAINE
NATIONAL AVIATION UNIVERSITY
DEPARTMENT OF AIRCRAFT DESIGN

APPROVED BY
Head of department Dr. of Sc., prof.
_____ Sergiy IGNATOVICH
"___" _____ 2022

MASTER THESIS

ON SPECIALITY
"AVIATION AND SPACE ROCKET TECHNOLOGY"

Theme: "Infrared nondestructive testing images research of glass fiber reinforced polymer composites"

Prepared by: _____ **Junjiang ZHOU**

Supervisor: D.Sc., professor _____ **Mykhailo KARUSKEVYCH**

Labor protection:
Ph.D., a**ssociate professor** _____ **Katerina KAZHAN**

Environmental protection:
Ph.D., associate professor _____ **Lesya PAVLYUKH**

Standard inspector:
Ph.D., associate professor _____ **Volodymyr KRASNOPOLSKYI**

Kyiv 2022

НАЦІОНАЛЬНИЙ АВІАЦІЙНИЙ УНІВЕРСИТЕТ

Факультет аерокосмічний
Кафедра конструкції літальних апаратів
Освітній ступінь «Магістр»
Спеціальність 134 «Авіаційна та ракетно-космічна техніка»
Спеціалізації «Обладнання повітряних суден»

ЗАТВЕРДЖУЮ
Завідувач кафедри д.т.н., проф.
_____ Сергій ІГНАТОВИЧ
«___» _____ 2022 р.

ЗАВДАННЯ

на виконання дипломної роботи студента

Цзюньцзян ЧЖОУ

1. Тема роботи «Дослідження зображень інфрачервоного неруйнівного контролю полімерних композитів, армованих скловолокном», затверджена наказом ректора від 05 жовтня 2022 року № 1861/ст.
2. Термін виконання проекту: з 06 жовтня 2022 р. по 30 листопада 2022 р.
3. Вхідні дані до проекту: зображення неруйнівного контролю, нейромережа, властивості полімерних композитів.
4. Зміст пояснювальної записки: аналіз проблеми дослідження інфрачервоних зображень неруйнівного контролю полімерних композитів, армованих скловолокном, алгоритм суперроздільності та алгоритм аналізу головних компонент, експериментальна перевірка.
5. Перелік обов’язкового матеріалу: пояснювальна записка з аналізом стану проблеми, зображення неруйнівного контролю, побудована модель нейронної мережі, презентація результатів.

6. Календарний план-графік:

№	Завдання	Термін виконання	Відмітка про виконання
1	Отримання завдання, обробка статистичних даних або аналіз сучасних ідей, концепцій, задумів.	05.10.2022 – 12.10.2022	
2	Організація та вивчення відповідних навчальних матеріалів.	13.10.2022 – 14.10.2022	
3	Написання першої частини дипломної роботи.	15.10.2022 – 28.10.2022	
4	Створення моделі нейронної мережі та навчання її для інфрачервоного неруйнівного контролю.	28.10.2022 – 10.11.2022	
5	Написання експериментальної та підсумкової частини дипломної роботи.	10.11.2022 – 21.11.2022	
6	Завершення дипломної роботи.	21.11.2022 – 30.11.2022	
7	Заповнення пояснювальної записки.	30.11.2022 – 05.12.2022	

7. Консультанти з окремих розділів

Розділ	Консультанти	Дата, підпис	
		Завдання видав	Завдання прийняв
Охорона праці	Катерина КАЖАН		
Охорона навколишнього середовища	Леся ПАВЛЮХ		

8. Дата видачі завдання: «06» жовтня 2022 р.

Керівник дипломної роботи _____ Михайло КАРУСКЕВИЧ

Завдання прийняв до виконання _____ Цзюньцзян ЧЖОУ

NATIONAL AVIATION UNIVERSITY

Faculty aerospace
Department of aircraft design
Master's degree
Specialty 134 "Aviation and space rocket technology"
Educational professional program "Aircraft equipment"

APPROVED BY
Head of department Dr. of Sc., prof.
_____ Sergiy IGNATOVICH
"___" _____ 2022

TASK
For the master thesis
Junjiang ZHOU

1. Topic "Infrared nondestructive testing images research of glass fiber reinforced polymer composites", approved by the Rector's order № 1861/ст of 5th October 2022.
2. Thesis terms: from 6th October 2022 to 30th November 2022.
3. Initial data: Non-destructive damage images, neural network, properties of polymer composites.
4. Content: analysis of the problem of infrared non-destructive testing images research of glass fiber reinforced polymer composites, super-resolution algorithm and principal component analysis algorithm, experimental testing.
5. Required material: explanatory notes with state of problem analysis, non-destructive damage images, built a neural network model, presentation of the results.
6. Thesis schedule:

№	Task	Time limits	Done
1	Obtaining the task, processing statistical data or analysis of contemporary ideas, concepts, designs.	05.10.2022 – 12.10.2022	

2	Organize and study related study materials.	13.10.2022 – 14.10.2022	
3	Writing the first part of the thesis.	15.10.2022 – 28.10.2022	
4	Build a neural network model and train it for infrared non-destructive testing.	28.10.2022 – 10.11.2022	
5	Writing the experimental and conclusion part of the thesis.	10.11.2022 – 21.11.2022	
6	Complete the thesis.	21.11.2022 – 30.11.2022	
7	Completion of the explanatory note.	30.11.2022 – 05.12.2022	

7. Special chapter consultants

Chapter	Consultants	Date, signature	
		Task issued	Task received
Labor protection	Katerina KAZHAN		
Environmental protection	Lesya PAVLYUKH		

8. Date: "06" October 2022

Supervisor of diploma work _____ Mykhailo KARUSKEVYCH

Task for execution is given for _____ Junjiang Zhou

РЕФЕРАТ

Магістерська робота «Дослідження зображень інфрачервоного неруйнівного контролю полімерних композитів, армованих скловолокном»

74 с., 22 рис., 7 табл., 80 джерел

З розвитком суспільства, науки та технологій у різних галузях промисловості висуваються все вищі вимоги до роздільної здатності зображень. Якщо роздільна здатність невисока, це може призвести до негативних наслідків і ускладнень для деяких робіт. Технологія реконструкції з надвисокою роздільною здатністю – це метод, який не потребує оновлення апаратного рівня для покращення роздільної здатності зображення. До появи методів глибокого навчання люди здебільшого використовували традиційні методи, такі як інтерполяція до зображень із надвисокою роздільною здатністю, але цей метод дуже обмежений. Згенеровані зображення також незадовільні, особливо в умовах великої кількості зображень, цей алгоритм не можна цілеспрямовано оновити й оптимізувати, а супер-роздільна здатність на основі глибокого навчання може добре вирішити цю проблему, але не всі методи супер-глибокого навчання мають чудові результати. Щоб вирішити цю проблему, у цій роботі пропонується алгоритм супер-роздільності, заснований на генеративних змагальних мережах.

Суперроздільна здатність, інфрачервоний неруйнівний контроль, генеративна змагальна мережа, полімерні композитні матеріали, скловолокно

ABSTRACT

Master degree thesis "Infrared nondestructive testing images research of glass fiber reinforced polymer composites"

74 p., 22 fig., 7 tables, 80 references

With the development of society, science, and technology, various industries have higher and higher requirements for the resolution of images. If the resolution is not high, it may bring negative effects and difficulties to some jobs. Super-resolution reconstruction technology is a method that does not need to upgrade the hardware level to improve image resolution. Before the advent of deep learning methods, people mostly used traditional techniques such as interpolation to super-resolution images, but this method is very limited. The generated images are also unsatisfactory, especially in the face of a large number of pictures, this algorithm cannot be upgraded and optimized in a targeted manner, and super-resolution based on deep learning can solve this problem well, but not all deep learning super-resolution methods have excellent results. In order to solve this problem, this paper proposes a super-resolution algorithm based on generative adversarial networks.

Super-resolution, infrared nondestructive testing, generative adversarial network, polymer composite materials, fiber-glass

CONTENT

PART 1. THE PROBLEM OF INFRARED NONDESTRUCTIVE TESTING IMAGES RESEARCH OF GLASS FIBER REINFORCED POLYMER COMPOSITES 11
1.1 Research background and significance 11
1.2 Research Status of Infrared Thermal Imaging Abroad 13
1.3 Research Status of Infrared Thermal Imaging in China 15
1.4 Traditional image super-resolution 17
1.4.1Interpolation based method 17
1.4.2Reconstruction based method 17
1.5 Image super-resolution based on deep learning 19
PART 2. SUPER-RESOLUTION ALGORITHM AND PRINCIPAL COMPONENT ANALYSIS ALGORITHM 20
2.1 Introduction 20
2.2 Image Interpolation Algorithm 22
2.2.1 Nearest Neighbor Interpolation Algorithm 22
2.2.2 Bilinear interpolation algorithm 23
2.2.3 Bicubic Interpolation Algorithm 24
2.3 Image super-resolution reconstruction technology based on deep learning 25
2.3.1 Residual block 25
2.3.2 Generative Adversarial Networks 26
2.3.3 Super-Resolution Reconstruction Based on Generative Adversarial Networks 28
2.4 Image Evaluation Methods 28
PART 3. SUPER RESOLUTION EXPERIMENT 31
3.1 Infrared test system 31
3.2 Experimental test block 32
3.3 Experimental procedure 33
3.3.1 Influence of motivation time 33
3.3.2 Influence of detection distance 36
3.4 Design and Construction of Super-Resolution Neural Network 38

3.4.1 Generator Design 38
3.4.2 Loss function 39
3.5 Super-resolution experiments 40
3.6 Experimental results 41
3.7 Infrared Nondestructive Testing Super Resolution Experiment 48
PART 4. LABOUR PROTECTION 51
4.1 Main production process and hazard factors 51
4.2 Harmful factors in glass fiber manufacturing 52
4.3 Analysis of working conditions and formulation of protective measures 56
4.4 Fire safety in the workplace 57
PART 5. ENVIRONMENTAL PROTECTION 59
5.1 Research progress of FRP waste recycling at home and abroad 61
5.2. Glass Fiber Recycling Methods 62
5.3 Glass fiber waste recycling method 64
REFERENCES 68

PART 1. THE PROBLEM OF INFRARED NONDESTRUCTIVE TESTING IMAGES RESEARCH OF GLASS FIBER REINFORCED POLYMER COMPOSITES

1.1 Research background and significance

Composite material is a new type of material composed of two or more different materials[1]; The advantages of various raw materials in performance are combined to produce a synergistic effect, which greatly improves the performance of the new composite materials. The parameters of the materials are far superior to those of raw materials. Matrix and reinforcement are two main components of composite materials. The matrix of glass fiber reinforced plastic (GFRP) is a synthetic resin, and its reinforcement materials are glass fiber and its products (glass cloth, tape, felt, etc.)[2].

Three kinds of inorganic non-metallic materials with excellent performance, also known as glass fiber reinforced plastics. Its main characteristics are small density, lightweight, good insulation, high strength, and good corrosion resistance. In general, the specific strength of glass fiber winding material (hereinafter referred to as glass fiber) is 4-5 times that of steel, so it is the preferred material for metal product substitutes[3]. Therefore, the excellent mechanical properties of composite materials make it widely used in vehicle filament wound gas cylinders, pressure vessels, pressure pipelines, and other industries that require high safety factors. At the same time, the safety performance of composite materials has become the focus of attention. The traditional GFRP defect detection methods include X-ray detection, acoustic emission, penetration, and ultrasonic detection[4]. Although X-ray testing is widely used at home and abroad.

During measurement, the radiation is harmful to the human body, and safety protection is required; Ultrasonic testing is easy to operate, but the operator must have practical experience, and the coupling agent and corresponding probe are required for testing; The penetrant method is simple and fast, but it requires penetrant oil and developer, which can only detect near surface defects and cannot detect internal defects; The operation of infrared thermal imaging and acoustic emission method is complex, in addition, additional pressure, heating or loading of materials are required; Therefore, it is particularly

important to find a simple and effective method to supplement and improve the traditional detection methods.

Because conventional nondestructive testing methods have their own characteristics and limitations[5], this promotes the rapid development of unconventional nondestructive testing, such as infrared thermal wave imaging testing technology. Infrared Thermography (IT) is a technology based on the principle of infrared radiation, which converts the infrared thermal radiation signal caused by surface defects or internal structure discontinuities of the tested piece into an electrical signal for easy analysis through an infrared thermal imager, thereby realizing the purpose of non-destructive testing[6]. In infrared thermal imaging nondestructive testing, due to the influence of environmental noise, uneven heating, etc., the infrared image may have a low signal-to-noise ratio, weak defect signal, and noise covering defect information. Therefore, further processing of infrared image sequences is required to eliminate noise interference, improve the signal-to-noise ratio, and enhance defect image information. At present, the commonly used infrared sequence image processing methods mainly include Thermal Signal Reconstruction (TSR), Lock in Thermography (LT), Pulse phase Infrared Thermography (PPT), Dynamic Thermal Tomography (DTT), and Likeness Optical Flow (LOF)[7]. Although the accuracy and robustness of the traditional infrared target detection algorithms have been improved in recent years, there are their own applicability and limitations. To sum up, there are the following points: First, it is difficult to extract complex features manually, and even if it can be successfully extracted, it is necessary to have some preliminary knowledge of the detected target; Secondly, the classification training of the extracted features is more complex, and the training effect highly depends on the feature extraction; Finally, the effect of the algorithm is closely combined with specific tasks, and the portability is poor. Different algorithms should be designed for different detection targets[8].

In recent years, deep learning has made remarkable achievements in many computer vision tasks. Convolutional neural network (CNN) has been widely used in image processing, image classification, target recognition, and other fields due to their strong feature extraction ability, generalization ability, and robustness to a certain degree of distortion[9]. The convolutional neural network has a strong ability for feature extraction and

generalization. Its application in infrared thermal imaging nondestructive testing will help to improve the detection accuracy and speed of existing algorithms. Among them, the deep learning algorithm has broad application prospects in infrared nondestructive testing. The purpose of deep learning is to build a statistical model based on data, which requires a large number of tag data training and has a good performance on super-resolution images.

Therefore, it has important theoretical research significance and practical application value to deeply discuss and study the traditional infrared sequence image super-resolution technology, as well as the super-resolution technology based on deep learning training optimization, to provide a technical security guarantee for solving the efficient and accurate identification and production operation of GFRP. This paper mainly studies the common defects of GFRP.

1.2 Research Status of Infrared Thermal Imaging Abroad

In the 1960s, foreign countries first began to research infrared nondestructive testing technology and applied it to defect detection of various metals, nonmetals, and composites[10]. In 1992, Almond D P et al[11]. of Bath University in the United Kingdom studied the infrared pulse thermal wave imaging method. Considering the influence of edge effects on the size of defects, they used the thermal conductivity of materials to extract the characteristics of character defects and named it the Wiener Hopf method. Since then, based on the development and improvement of the infrared pulse thermal wave imaging method, academia has successively proposed dynamic thermal tomography, infrared phase-locked thermal wave imaging, infrared pulse phase method, thermal signal reconstruction method, similar optical flow method, and other methods. In terms of dynamic thermal chromatography, Vavilov V et al. of the Tomsk University of Technology, Russia, initially proposed a method to obtain defect depth information from image sequences of temperature changes under pulse excitation in 1990 and named it Dynamic Thermal Tomography (DTT) for the first time[12],[13]. In 2012, Melnyk S, et al. of the Radio and Electronics University of Ukraine proposed the Projection Dynamic Thermal Tomography (PDTT), which improved the dynamic thermal chromatography by using the three-dimensional thermal reconstruction algorithm to make the surface emission capacity of the measured object more uniform[14].

In 2018 Vavilov V et al. believed that in anisotropic composites, heat is more easily diffused in one direction than in the other, and transverse diffusion makes it difficult to detect shallow defects[15]. Therefore, he improved the dynamic thermal chromatography, proposed to use the principle of unilateral thermal imaging to detect 34J impact damage energy in a 6mm thick carbon fiber cloth sample, and used the thermal stratification method to calibrate the material layer in one dimension. The experimental results show that the method has significantly improved the detection effect of shallow defects. In terms of the infrared phase-locked thermal wave method, Busse G of the University of Stuttgart, Germany, first proposed the infrared phase-locked thermal wave method (LT) in 1992 [16]. Compared with the conventional infrared detection technology, this technology can increase the depth range required for imaging in a short time. In 2005, Meola C, et al. of Federico II University in Naples, Italy, used the infrared phase-locked thermal wave method to carry out an experimental analysis on common damage types in aviation material structures[17]. The results show that the infrared phase-locked thermal wave method can be effectively used to detect the defect size of composite materials and the expansion range of impact damage of composite materials. In 2019, Shrestha R et al. of Kongzhou National University in South Korea used the infrared phase-locked thermal wave method to detect the water inflow of aircraft HSCs and studied the influence of water content on quantitative estimation[18]. The results show that the principal component analysis method is superior to Fourier transform and harmonic approximation qualitatively, and the principal component analysis method can obtain the highest signal-to-noise ratio quantitatively. In 2020, Oliveira B, et al. of the Federal University of Santa Catalina in Brazil proposed to characterize the impact damage of carbon fiber reinforced material plates by image fusion of optical lock-in thermography (OLT) and optical square pulse shearing (OSS)[19]. The results show that the measurement error of equal diameter is reduced by 72.21%, and the measurement is enhanced by 8.05%. The fusion method can effectively detect impact damage.In terms of the infrared pulse phase method, Maldague X et al. of Laval University in Canada extracted different frequency domain information in pulsed infrared thermal images through Fourier transform in 1995[20]. Combining the advantages of modulation and pulsed infrared thermal images, they proposed the infrared pulse phase method (PPT). In 2013, Austrian researcher Gruber J et al. used the

infrared pulse phase method to detect carbon fiber skin HSCs and evaluated the impact of measurement time and the feasibility of extrapolating temperature attenuation[21]. The experimental results show that compared with ultrasonic testing, the infrared pulse phase method can reduce the actual measurement value by using the extrapolation principle to improve detection accuracy. In 2018, Popow V et al. of the German Composite Research Institute used the infrared pulse phase method to detect the defects of carbon fiber-reinforced composites[22]. The experiment showed that the inhomogeneity and anisotropy of the composite caused by the microstructure of the defects had an important impact on the detection accuracy. In 2003, Shepard S of American TWI Company proposed to convert the temperature-time data of each pixel in the obtained infrared image into the log domain, perform least square fitting on the data, detect defects by observing the zero crossing characteristics of the second derivative of the polynomial corresponding to the temperature time data of a given pixel, and name this method Thermal Signal Reconstruction (TSR) [23,24]. In 2013, Oswald T et al. of Leoben University, Austria used the thermal signal reconstruction method to analyze the data sequence of optical pulse and scanning induction heating, proposed finite element simulation models with different diameters and depths, and discussed the impact of size measurement accuracy and noise on detection limit and sensitivity[25]. In 2015, Roche J of Aerosp Laboratory in France proposed a two-step pulse thermal imaging experimental data processing method for thermal D-scanning of composite materials and structures. The results show that the method can be applied to the actual damage caused by the machining process or external work (such as impact, high temperature, or quasi-static mechanical load) by verifying the quantitative imaging of calibration defects with known depth[26].

1.3 Research Status of Infrared Thermal Imaging in China

In China, researchers from various universities have also conducted a lot of research on infrared nondestructive testing. In 2007, Xu Chuan of Capital Normal University and others studied the data processing methods in the phase-locked thermal imaging detection system, including dual channel digital phase-locked, Fourier transform, etc[27]. They also studied the influence of periodic square wave heating on the experiment and discussed the

principle, implementation method, and problems to be noticed in the experiment of phase-locked thermal imaging technology. In 2008, Jiang Qianhui et al[28]. of Capital Normal University used the region growth algorithm based on local minimum to extract defects in the pulse thermal imaging detection image. In the same year, Li Yanhong[29] of Beijing University of Technology and others conducted pulse phase analysis on aluminum specimens with flat bottom holes to obtain phase images at different frequencies, effectively suppressing noise interference. In 2009, Zhan Shaozheng of AVIC Aircraft Strength Research Institute and others conducted a comparative test of pulse thermal imaging and phase-locked thermal imaging on composite honeycomb sandwich structure specimens[30]. The results show that the image quality obtained by phase-locked thermal imaging is higher. In 2012, Liu Junyan of Harbin University of Technology and others carried out a lot of work on various specimens, including SiC coating and carbon fiber composites, using phase-locked thermal imaging methods, and proposed a variety of feature information extraction algorithms and technologies[31-33]. In the same year, Liu Tao of the Second Artillery Engineering University and others introduced BP neural network [34]into the data post-processing process of phase-locked thermal imaging to achieve quantitative identification of defects. In 2013, Tang Qingju et al. of Harbin Institute of Technology respectively used temperature time logarithmic fitting, principal component analysis, and pulse phase method to extract the characteristic information of the thermal wave signal generated by the thermal pulse. Among them, the demodulation result of principal component analysis has a high signal-to-noise ratio. In 2016, Zhou Zhenggan, et al[35]. of Beijing University of Aeronautics and Astronautics established a finite element model for phase-locked infrared thermal imaging detection of titanium alloy honeycomb structures and obtained the optimal frequency of phase-locked thermal imaging detection from simulation calculations. In 2019, Wang Zhen, et al[36]. of Rocket Army University of Engineering proposed a post-processing method of phase-locked thermal imaging data based on phase-shifting technology. It was proved through experimental comparison that the new technology improved the ability to identify small defects and improved the contrast of results.

In 2019, Wei Jiacheng, et al[37]. of Harbin University of Technology applied the Likeness Optical Flow (LOF) method to infrared thermal wave imaging detection, reducing

the transverse thermal diffusion effect of materials and improving the accuracy of defect detection.

1.4 Traditional image super-resolution

1.4.1Interpolation based method

There is a correlation between adjacent pixels of the original image, and the interpolation-based method effectively uses this correlation to complete image SR. This method can also have a good effect when training samples are insufficient. Generally, it can be subdivided into nearest neighbor interpolation, bilinear interpolation, and bicubic interpolation. Nearest neighbor interpolation can be described as when the image is enlarged, the missing pixel directly copies the nearest pixel with its color similar to it to generate a new image. The image generated by this method will generate a sawtooth, and the reconstruction effect is general. The bilinear interpolation method does not directly use adjacent pixel values but performs linear interpolation in two directions within the four neighborhoods where pixels are missing. This method requires more computation than the nearest neighbor interpolation method. The results are usually not linear, but there is no sawtooth like the nearest neighbor interpolation method, and the results are good. However, due to its low-pass filtering characteristics, it is unable to retain more high-frequency information from the original image, so the image outline will be slightly blurred. Bicubic interpolation is the most commonly used interpolation method in two-dimensional space. The pixel value of a point is obtained by weighting the pixel values of 16 sampling points around the rectangular grid of space. In 2D image space, two polynomials are usually used to interpolate cubic functions. Therefore, this method is better than the SR method based on interpolation, and it is often used to compare with the deep learning method[38].

1.4.2Reconstruction based method

The prior knowledge is very complex, but image SR must use it as a constraint to generate HR images. A priori knowledge improves the performance of linear models, making reconstruction-based methods more advantageous in generating clear and sharp details. Based on the reconstruction method, the acquisition process of the LR image is

modeled, the prior constraint conditions of the HR image are constructed, SR is transformed into cost function optimization with constraint conditions, and ill condition problem is transformed into a good condition problem. Usually, manually defined smoothing constraints on HR images are regarded as prior knowledge.

1) Iterative back projection method

Iterative Back Projection (IBP) was put forward in 1991. It is the operation of the back projection of LR images to establish the mapping between LR and HR images. Although there will be some error sets, the corresponding HR image will be obtained finally. Later, Tom and others introduced an improved motion compensation method and applied it to single image SR based on the IBP algorithm[39]. The algorithm is not only intuitive and simple but also has significantly improved performance. It is also extended to video sequence super-resolution reconstruction to achieve a wider application.

2) Projection method of a convex set

Although the IBP algorithm has obvious advantages, it is difficult to use prior information and the solution to the problem is not unique. In 1989, Stark et al[40]. Then in 1998, Patti et al[41]. proposed a POCS method that can include additive noise, which not only solves the problem of motion blur but also considers the limitations of aliasing and sensor blur on SR. In the POCS algorithm, a constraint convex set can be defined by a similar constraint condition such as the boundedness of nonnegative energy in the very limited solution region of SR, and then the intersection set of the forced constraint set with HR image property is calculated to obtain the solution space iteratively. POCS overcomes the weakness of the IBP algorithm without prior information, maintains the edge and detail features of HR image, and promotes the development of image SR to a certain extent.

3) Adaptive filtering method

POCS algorithm has the disadvantages of low convergence stability and a large amount of computation while adding prior information. Although the relaxation projection operator can improve, image edges and details will not be maintained. In 1999, Elad et al. proposed to realize SR based on the recursive steepest descent method and recursive least mean method. In 2000, Alam et al. improved the filtering[42]. In 2007, Naratana et al[43]. This

method can preserve the edge and detail features of the image, but it can not contain prior knowledge, especially nonlinear prior knowledge.

1.5 Image super-resolution based on deep learning

Before the advent of convolutional neural networks, the key to the image SR problem was to share feature information between LR images and HR images. The previous methods for the use of this information are not complete, resulting in the image contour texture expression is not very sufficient. Since the convolutional neural network was applied to computer vision, various SR methods based on deep learning have emerged. The CNN model consists of three parts: feature extraction, nonlinear mapping, and feature reconstruction. Convolution plays an important role in these three parts. The advantage of CNN is that it is simple to express mathematically and can complete the SR of images through joint training. It can be seen that deep learning is more suitable for application in the field of single image super-resolution reconstruction[44].

Conclusion for part 1.

1. The development status of infrared nondestructive testing at home and abroad is introduced.
2. The traditional super-resolution method and the super-resolution algorithm based on deep learning are introduced.
3. The research of super-resolution method by domestic and foreign scholars is briefly summarized.

PART 2. SUPER-RESOLUTION ALGORITHM AND PRINCIPAL COMPONENT ANALYSIS ALGORITHM

2.1 Introduction

With the development and progress of nondestructive testing, conventional nondestructive testing technology has become more and more perfect, and its scope of application has become wider and wider. From the beginning, it was only applied to the military industry, and aerospace industry, and now it has become an indispensable gear in the development system of the industrial era. Representative nondestructive testing includes ultrasonic testing (UT), radiographic testing (RT), electromagnetic testing (ET), magnetic particle testing (MT), and penetrant testing (PT),these classical methods have their own strengths and limitations[45].

Although the five routine tests have developed very mature at present, the emerging nondestructive testing technologies such as infrared testing have been widely concerned by researchers because of their unique advantages such as fast detection speed, no contact, and no harm to human health. However, although the infrared nondestructive testing technology has unique characteristics, its own defects are also very obvious. For example, the imaging effect of an infrared image is affected by the performance parameters such as the resolution and sensitivity of the infrared camera itself, and at the same time, it is easy to be influenced by external factors such as background radiation, noise, etc. The final image effect is not good, such as low contrast, blur, and low level of detail, so the defect representation level is reduced, and the imaging effect of the infrared image directly affects the defect detection effect of infrared nondestructive testing. Therefore, for infrared images, the defect detection effect of infrared nondestructive testing is very low. Therefore, it is a very important step to optimize the infrared image. Image interpolation has always been a hot topic in the image field. The main purpose of the algorithm is to estimate the unknown pixel

information by using the known pixel information, so as to interpolate the low-resolution image into the corresponding high-resolution image, thus improving the visual effect. There are two main types of methods to increase:

(1) Improve the resolution by upgrading the hardware level of equipment.

(2) Super-resolution is performed on the existing low-resolution images by software or algorithm to obtain high-resolution images.

However, at present, it is not practical to improve the resolution by upgrading the hardware, because the cost of upgrading the equipment is very high, and there is no way to break through the upper limit due to the limitation of the current hardware specification, so the super-resolution method using the algorithm is more feasible.

Aiming at the problems of low resolution and low level of detail of infrared imaging images, this paper will use the traditional image interpolation algorithm, principal component analysis, and super-resolution algorithm based on deep learning to process infrared images.

The main research contents of this paper are as follows:

(1) The nearest neighbor interpolation, bilinear interpolation, and bicubic interpolation algorithms are used to interpolate images, and the super-resolution effect of traditional methods on images is explored.

(2) The principal component analysis method is used to process the infrared image, and the optimization effect of this method on the infrared image is studied and analyzed.

(3) Finally, the model of generative adversarial super-resolution network based on deep learning is built, trained and super-resolution experiments are carried out, and the advantages and limitations of super-resolution algorithm based on deep learning and traditional super-resolution algorithm are analyzed.

2.2 Image Interpolation Algorithm

2.2.1 Nearest Neighbor Interpolation Algorithm

Nearest neighbor interpolation, also known as zero-order interpolation, is the easiest interpolation algorithm to realize, and its operating speed is also the fastest. The main realization method is to use the gray value of the nearest neighbor with the shortest Euclidean distance among the four neighboring pixels around the pixel to be estimated as the input gray value of the pixel[46].

Calculation formula of nearest neighbor interpolation coordinate transformation:

$$srcX=dstX*(srcWidth/dstWidth) \quad (2.1)$$

$$srcY=dstY*(srcHeight/dstHeight) \quad (2.2)$$

dstX and dstY: the horizontal and vertical coordinates of a pixel of the target image

dstWidth and dstHeight: the length and width of the target image

srcWidth and srcHeight: the width and height of the original image

srcX, srcY: the coordinates of the original image corresponding to the target image at this point (dstX, dstY)

Assuming that the left image is the original image, the right image is the enlarged target image as shown in fig. 2.1, the coordinates of the unknown point are (3,2), srcX=3*(2/4)=1.5, srcY=2*(2 /4)=1; so the pixel at the unknown point should be the value of the (1.5,1) pixel in the original image, but the pixel coordinates do not have decimals, generally rounding is used to get the nearest neighbor, so the final result is (2.1) , which corresponds to the pink color of the original image. Other analogies get the enlarged image as shown in fig. 2.2:

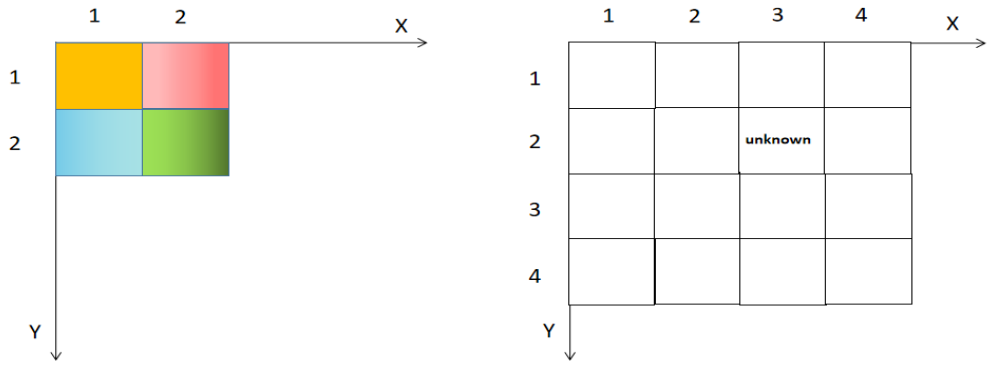

Fig. 2.1.

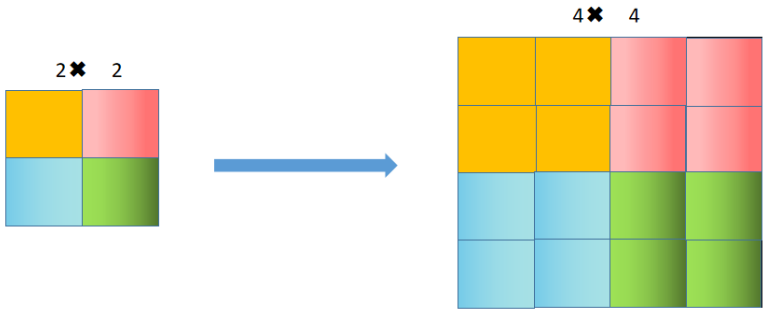

Fig. 2.2.

2.2.2 Bilinear interpolation algorithm

Bilinear interpolation algorithm, also known as first-order interpolation, is proposed to improve the fuzzy problem of nearest neighbor interpolation algorithm after interpolation[47-49].Different from the nearest neighbor interpolation, the principle of bilinear interpolation is linear interpolation in two orthogonal directions based on the level of four-pixel values adjacent to the pixel to be predicted, that is, the corresponding weights are determined according to the distance between the pixel to be predicted and the adjacent four pixels, so as to generate new pixels different from the original image.

Calculation formula of bilinear interpolation algorithm:

First, linear interpolation is performed twice in the X direction, and then interpolation is performed once in the Y direction.Similarly, when interpolating the image, the position of the new pixel in the original image is calculated according to the calculation formula of the nearest neighbor interpolation algorithm.

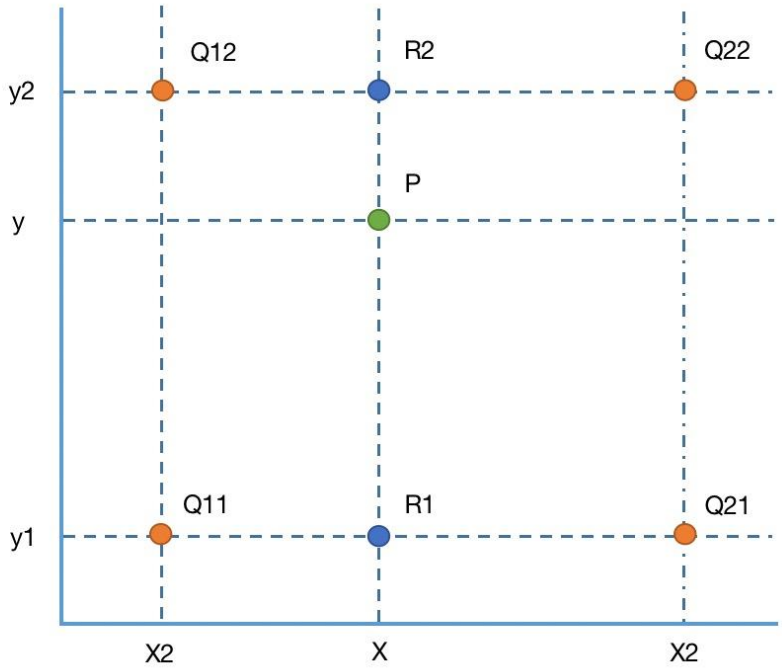

Fig. 2.3. Bilinear interpolation diagram.

$$f(x,y_1) \approx \frac{x_2-x}{x_2-x_1} f(Q_{11}) + \frac{x-x_1}{x_2-x_1} f(Q_{22}) \quad (2.3)$$

$$f(x,y_2) \approx \frac{x_2-x}{x_2-x_1} f(Q_{12}) + \frac{x-x_1}{x_2-x_1} f(Q_{22}) \quad (2.4)$$

$$f(x,y) \approx \frac{y_2-y}{y_2-y_1} f(x,y_1) + \frac{y-y_1}{y_2-y_1} f(x,y_2) \quad (2.5)$$

2.2.3 Bicubic Interpolation Algorithm

Bicubic interpolation also known as cubic convolution interpolation[50-54], this algorithm is different from bilinear interpolation algorithm in that it makes use of the pixel values of 16 pixels around the pixel to be predicted. Like Bicubic interpolation algorithm, it not only takes into account the pixel values of four adjacent pixels, but also takes into account the change rate of pixel values of adjacent pixels. This algorithm also needs interpolation function to fit the data. The most commonly used interpolation function is Bicubic basis function, so that a super-resolution image closer to the original image can be obtained, but compared with the first two algorithms, the amount of data calculation of the computer is greatly increased.

$$W(x)=\begin{cases}(a+2)|x|^3-(a+3)|x|^2+1 & for\ |x|\leq 1\\ a|x|^3-5a|x|^2+8a|x|-4a & for\ 1<|x|<2\\ 0 & otherwise\end{cases} \tag{2.6}$$

2.3 Image super-resolution reconstruction technology based on deep learning

2.3.1 Residual block

Theoretically speaking, the performance of the neural network model is proportional to the depth, that is to say: the more layers of the neural network, the better the performance of the network model will be, but the actual experimental results are not completely consistent with this rule, on the contrary In some cases, the performance of a network model with more layers is worse than that of a network model with fewer layers. In short, the performance of the network model is degraded, and even gradient explosion or gradient disappearance occurs, making the model unable to Moving on to deeper training, in order to solve this problem, a BN layer can be used to normalize the data. He[55] et al. proposed that the ResNet of the residual network uses a structure called residual network. The implementation method is to add channels directly connected to non-adjacent layers to the structure of the general convolutional neural network. One end of the network is directly connected to another layer across several layers. Experiments have shown that this structure has a very positive impact on the results of deep network training. The residual block network (right) and the basic network structure (left) are shown in fig. 2.4. It can be seen that the residual block network has a significant difference compared to the ordinary network structure, that is, the target changes from f(x) to f(x)-x, which means that the target changes from learning the input of the entire network structure to learning the input The difference between the output and the output greatly simplifies the computational complexity, and the residual network implements the identity mapping, which can make the

performance of the deep network not decrease due to the increase of the number of layers.

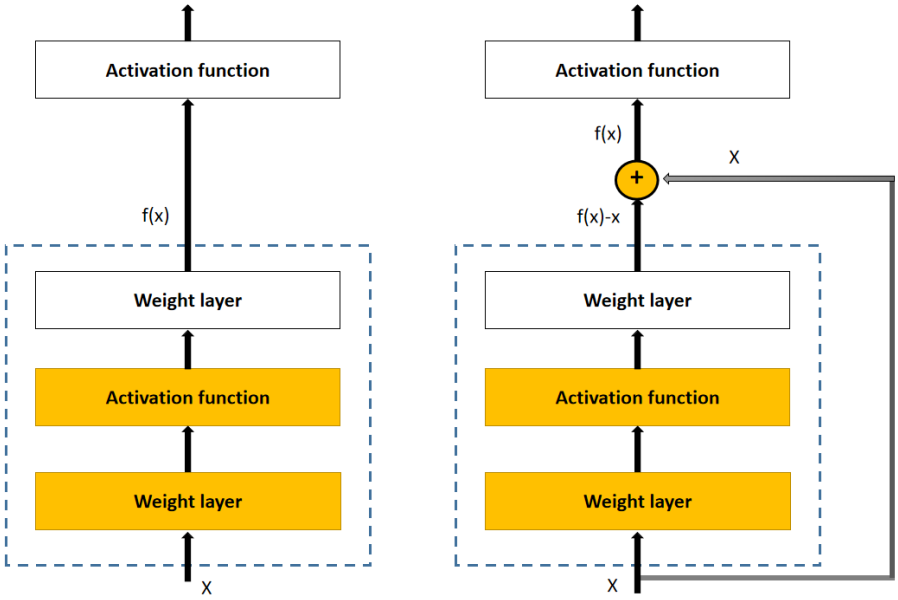

Fig. 2.4. Network structure.

2.3.2 Generative Adversarial Networks

The Generative Adversarial Network was first proposed by Goodfellow. This network structure is different from the traditional network. The Generative Adversarial Network has received the idea of game theory, and its core comes from Nash equilibrium, so there are two different branch structures in the network structure: generation G and discriminator D. During the training process, the generator G competes with the discriminator D. The selections of G and D are determined based on the optimal conditions. The training balance of G and D revolves around the numerical value of the loss function, which is a prerequisite for Nash equilibrium. In the next step, the confrontation between G and D will minimize the value of the loss function as soon as possible, and use this as the target for circular training until the value of the loss function can no longer be small. In the early stage of training, due to the small number of training times of the generator G, the generated data is not the optimal solution, which makes it easy for the data to be judged as false by the discriminator D, and as

the number of training times of the generator increases, the generated data It is getting closer and closer to the real value, making it difficult for the discriminator D to judge, and then giving the discriminant result as true. During the training process, the generator G will try to improve its ability to generate close to the real value, and the discriminator D also It will enhance its ability to discriminate data, and then make the confrontation between the two tend to be Nash equilibrium. A schematic diagram of the training process is shown in fig. 2.5.

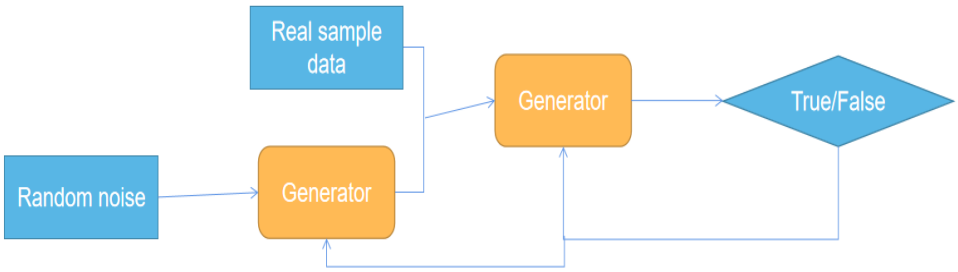

Fig. 2.5. Schematic diagram of the training process.

In the generative adversarial network for image super-resolution, the input is an image, and the output is a super-resolution image. With the increase of the number of generator training, the generator can generate a super-resolution image that is closer and closer to the original image. So that the discriminator judges it as the original image, which fulfills the requirements of image super-resolution.

Optimization objective function formula:

$$min_G max_D V(D,G) = E_{x\sim p_{data}(x)}[log(D(x))] = E_{z\sim p_z(z)}[log(1-D(G(z)))] \quad (2.7)$$

MinG: Generator Minimum Optimization Function

MaxD: discriminator maximum optimization function

x~pdata(x): real sample data

z~pz(z): random noise

D(x): Discriminant probability of real data

G(z): Probability of generating sample discrimination

2.3.3 Super-Resolution Reconstruction Based on Generative Adversarial Networks

The use of GAN for image super-resolution applications was first proposed by Ledig[56]. The input of the network is a low-resolution image, and the output is a high-resolution image output by the generator. With the increase of training times, the higher the number of high-resolution images generated by the generator is. It is getting closer to the original high-resolution image, so that the discriminator discriminates the super-resolution as the original image, which proves that the quality of the image generated by the generator is excellent, so as to achieve a good super-resolution target. The SRGAN structure is shown in fig. 2.6.

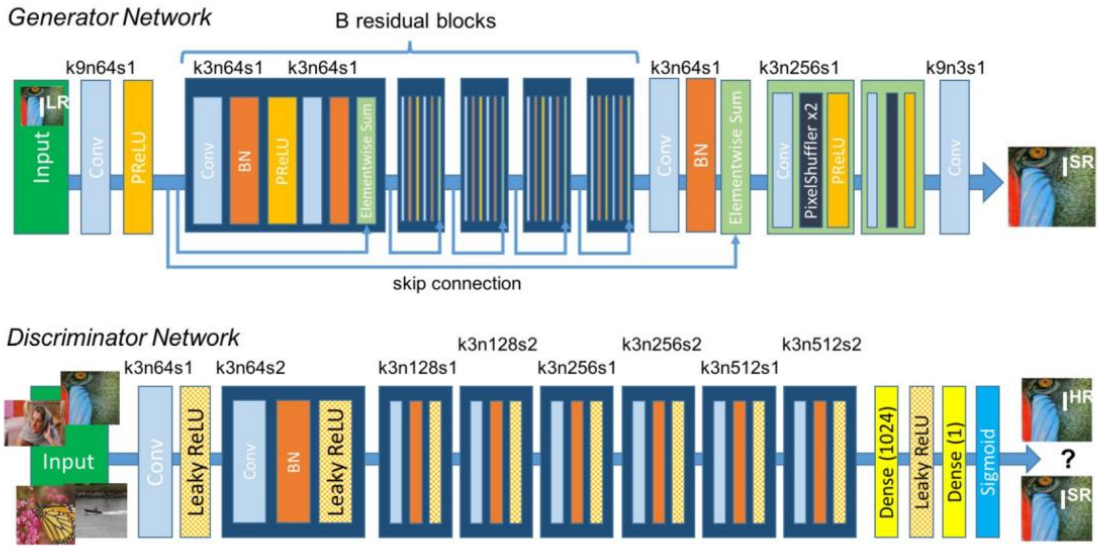

Fig. 2.6. Architecture of Generative and Discriminator Network.

2.4 Image Evaluation Methods

Image quality evaluation consists of subjective evaluation[57-58] and objective evaluation[59-63]. Subjective evaluation is mainly based on human eyes, which evaluates

images on the level of human vision and perception. This evaluation method is very intuitive, convenient and fast. However, because everyone's vision is not completely consistent, it is easily influenced by subjective factors, which leads to different people's evaluation of the same image and the possible results are not completely consistent. Objective evaluation is mainly based on the calculation of image data, which is not affected by other factors, and the results can basically be consistent. It is a widely used image evaluation method, but it also has its limitations.

Common subjective evaluation methods of image super-resolution:

MOS(Mean Opinion Score):

This is a subjective evaluation method, in which several evaluators score the image quality, and finally get the average value as the score of the image quality. This method is different from the objective evaluation method, and MOS can better reflect the details of image reconstruction to a certain extent, which is irreplaceable by the objective evaluation method. The disadvantage is that many evaluators are required to evaluate the image, and it is not conducive to adjusting parameters.

$$MOS = \frac{\sum_{i=1}^{k} n_i c_i}{\sum_{i=1}^{k} n_i} \tag{2.8}$$

PSNR(Peak Signal to Noise Ratio):

$$PSNR = 10log_{10}\left(\frac{MAX^2}{MSE}\right) \tag{2.9}$$

$$MSE = \frac{1}{H \times W}\sum_{i=0}^{H-1}\sum_{j=0}^{W-1}(x(i,j) - y(i,j))^2 \tag{2.10}$$

MAX: the maximum value of image point color.

SSIM(Structural Similarity):

This is an objective evaluation method. PSNR gives an objective evaluation at the pixel value level, and SSIM gives an objective evaluation of image structure, contrast, and brightness.

$$SSIM(x,y) = \frac{(2\mu_x\mu_y + c_1)(2\sigma_{xy} + c_2)}{(\mu_x^2 + \mu_y^2 + c_1)(\sigma_x^2 + \sigma_y^2 + c_2)} \tag{2.11}$$

$\boldsymbol{\mu_x}$: mean of x

μ_y: mean of y

σ_{xy}: covariance of x and y

σ^2_x: variance of x

σ^2_y: variance of y

c_1: *constant used to maintain stability*

c_2: *constant used to maintain stability*

$c_1=(k_1L)^2$, $k_1=0.01$

$c_2=(k_2L)^2$, $k_2=0.03$

Conclusion for part 2:

This chapter introduces the interpolation algorithm, deep learning-based adversarial generation network image super-resolution algorithm used in the experiment to lay a solid foundation for the experiment. The main contents are as follows:

1. Introduce the nearest neighbor interpolation algorithm, bilinear interpolation algorithm, bicubic interpolation algorithm.

2. Combined with adversarial generative network, the image super-resolution algorithm based on generative adversarial network is introduced.

3. The subjective and objective image evaluation methods of images are introduce.

PART 3. Super Resolution Experiment

3.1 Infrared test system

The infrared nondestructive testing experimental system of this subject is mainly composed of thermal excitation source, infrared camera, data synchronization acquisition system, and computer. The infrared camera model is VarioCAM HD980 The thermal excitation source is four halogen lamps with a power of 500W watts. During the experiment, a halogen lamp will be used to heat the test block, and then an infrared thermal imager will be used to record the temperature change of the test block. The schematic diagram of the experiment is shown in Figure 3.1, and the experimental setup is shown in fig. 3.2.

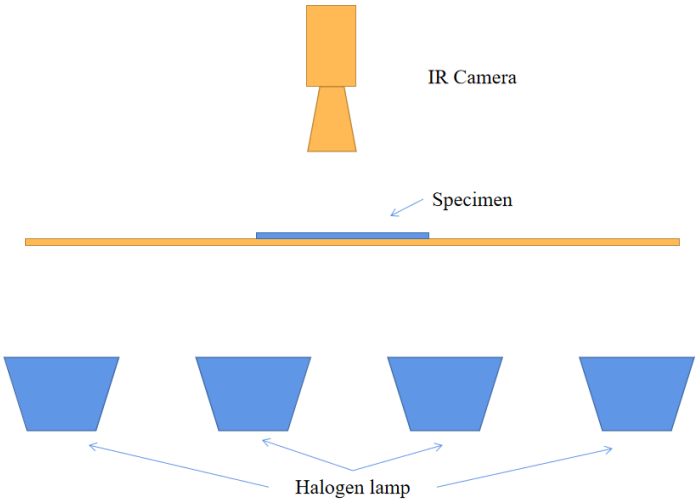

Fig. 3.1. Schematic diagram of the experiment.

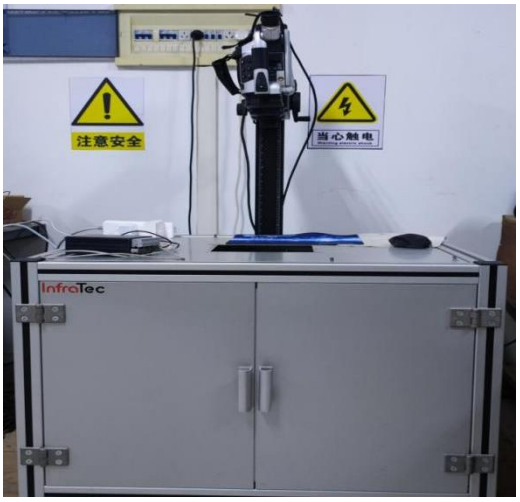

(a)Test system

(b) Infrared camera

Fig. 3.2. Experimental setup.

3.2 Experimental test block

The material of the test block is glass fiber, the defect is designed as a flat-bottomed hole, the size is 200×300×10 mm, the size of 6 defects is the same, and the burial depths are 4 mm, 5 mm, 6 mm, 7 mm, 8 mm, 9 mm respectively. The schematic diagram of the test block is shown in fig. 3.3. The test block diagram is shown in fig. 3.4.

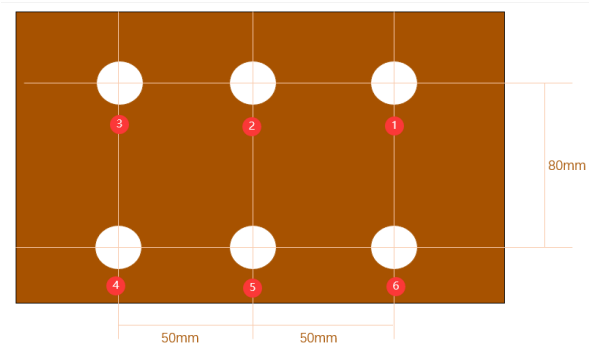

Fig. 3.3. Schematic diagram of the test block.

Fig. 3.4. Test block diagram.

3.3Experimental procedure

3.3.1Influence of motivation time

The thermal excitation time of infrared non-destructive testing has a relatively significant impact on the detection effect. Different excitation times will cause different detection results. If the excitation time is too short, the heating effect of the test block may not be obvious, and the temperature difference between the defect and the intact area is small, which makes it difficult to Defects are detected, but too long excitation time will also causes problems, which may lead to excessive thermal diffusion of the test block, and the thermal diffusion will cover up the defect signal, which also makes it difficult to detect defects. Therefore, it is necessary to choose the best excitation time.

During the experiment, the detection distance was set to 55 cm, the acquisition frequency was 10 HZ, the number of acquisition frames was 800 frames, and the excitation time was set to 5 s, 10 s, 15 s, 20 s, 25 s, and 30 s, respectively.

The more significant the temperature difference between the defect and the intact area, the better the defect can be reflected on the infrared image. Therefore, the value of the temperature difference can be used to preliminarily evaluate the detection effect.

Temperature difference formula:

$$Q_c = \bar{Q}_1 - \bar{Q}_2 \tag{3.1}$$

$\bar{Q}_1$: Take the center position of six flat-bottom hole defects to find the average temperature, in °C;

$\bar{Q}_2$: Randomly select six points in the non-defective area to obtain the average temperature, in °C;

$\bar{Q}_c$: The temperature difference between the defect area and the non-defect area, in °C.

Find the corresponding temperature change curve and draw it in the same coordinate system, as shown in fig. 3.5, the test results are shown in fig. 3.6.

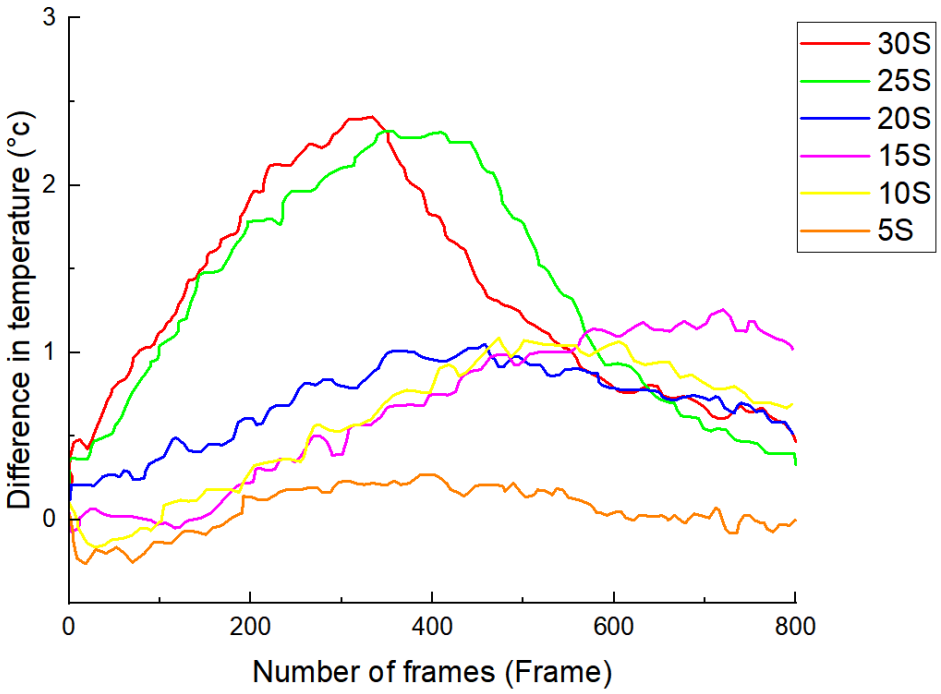

Fig. 3.5. Temperature difference curve.

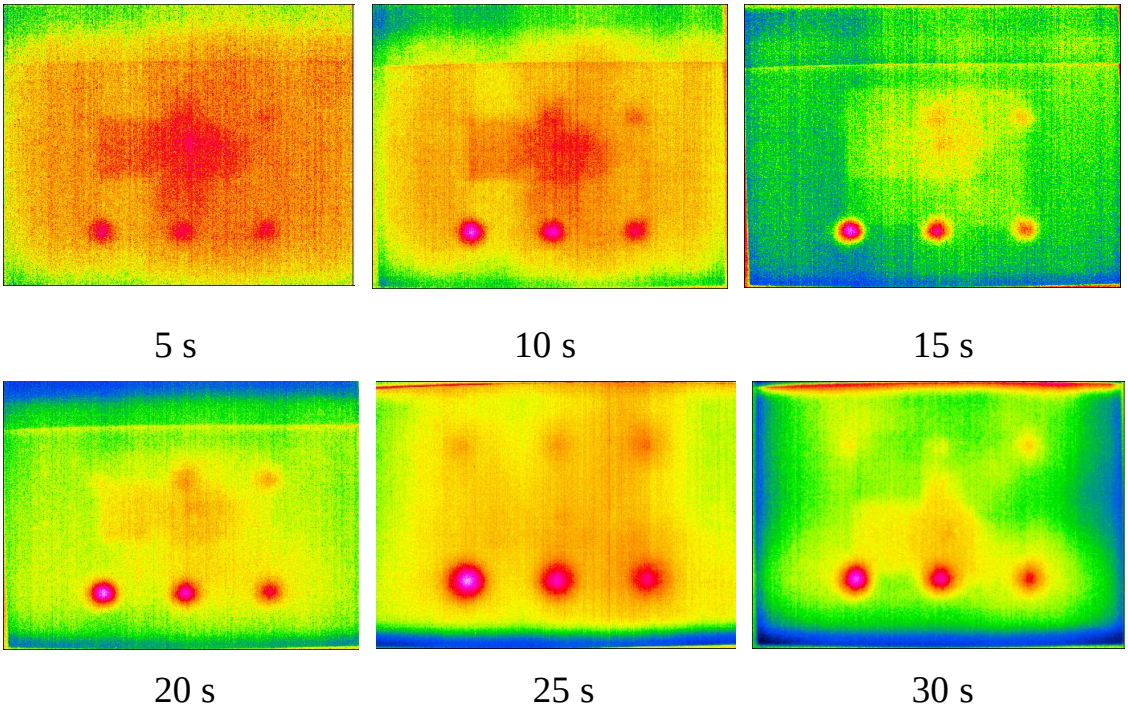

Fig. 3.6. Comparison of different heating times.

According to the temperature difference curve, it can be seen that the temperature difference is the largest when the excitation time is 30 s, the temperature difference of 25 s exceeds 2 degrees Celsius, and the duration is longer, so the excitation time of 25 s is selected as the best excitation time.

Comparing the infrared images obtained with different excitation times, select the frame with the largest temperature difference for comparison. It can be seen that the excitation time of 25 s and 30 s can detect all the defects. The images were compared using the peak signal-to-noise ratio (PSNR), and the drawn images are shown in fig. 3.7.

From fig. 3.7, it can be concluded that as the excitation time increases, the peak signal-to-noise ratio of the infrared image gradually increases until it reaches the best at 25 s, and begins to decline at 30 s, so 25 s is the best excitation time, and the experiment will also use 25 s as the excitation time.

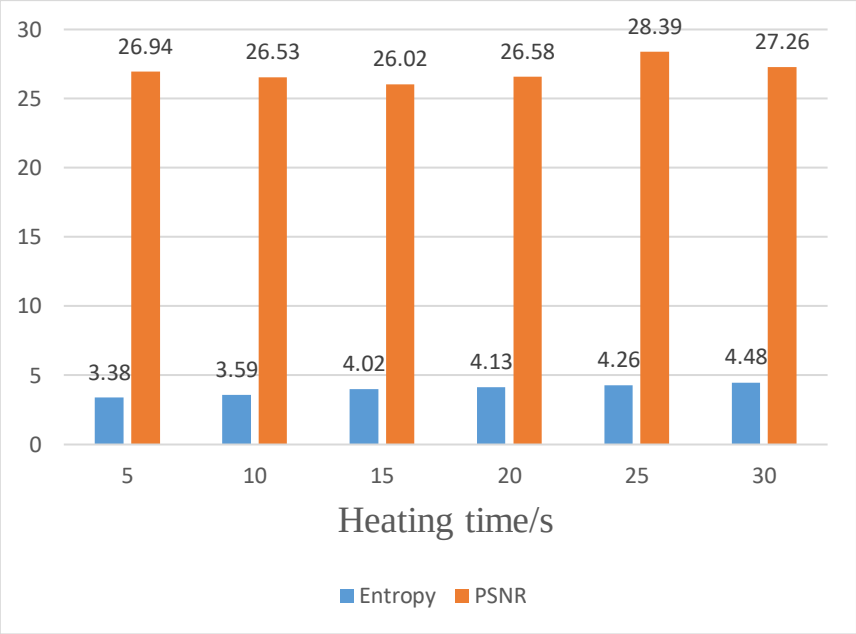

Fig. 3.7. PSNR Results.

3.3.2 Influence of detection distance

According to the theory of thermal radiation, the magnitude of thermal radiation is related to the distance. The farther the distance is, the greater the attenuation of thermal radiation. Therefore, the detection distance also affects the infrared detection effect, so it is equally important to choose the best detection distance. During the experiment, the detection distances were set to 30 cm, 35 cm, 40 cm, and 45 cm, respectively. The temperature curves at different detection distances are obtained through experiments, as shown in fig. 3.8, the test results are shown in fig. 3.9.

As can be seen from fig. 3.8, when the detection distance is 30 cm, the peak temperature difference is the largest, and as the detection distance increases, the peak value of the temperature difference curve gradually decreases. The results were evaluated using peak signal-to-noise (PSNR) and the results are shown in fig. 3.10.

From fig. 3.10, it can be concluded that when the detection distance is 35 cm, the peak signal-to-noise ratio is the highest, and the detection distance of 35 cm is selected as the best detection distance. The subsequent experiments will also use 35 cm as the detection distance.

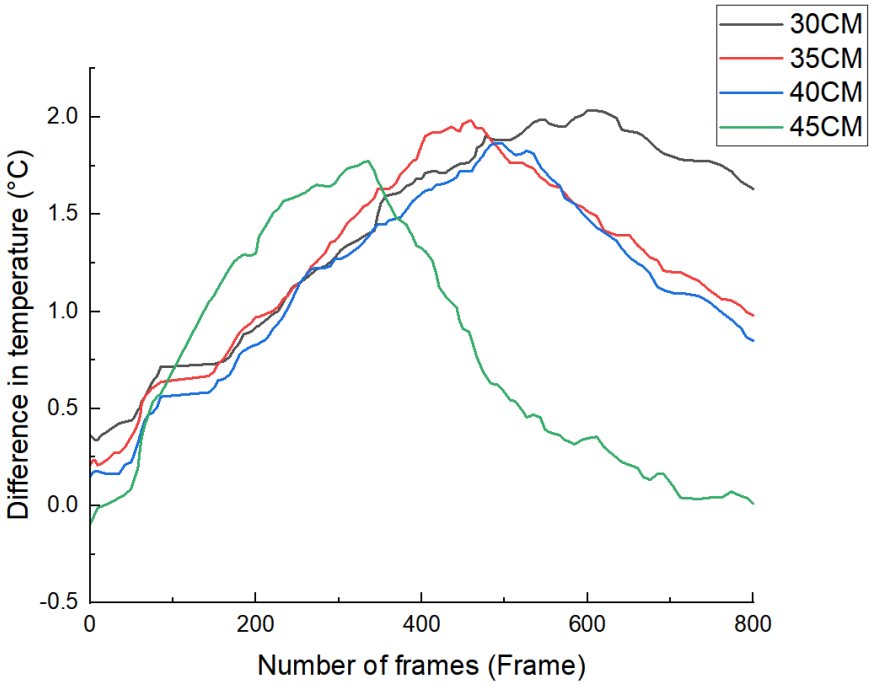

Fig. 3.8. Temperature difference curve.

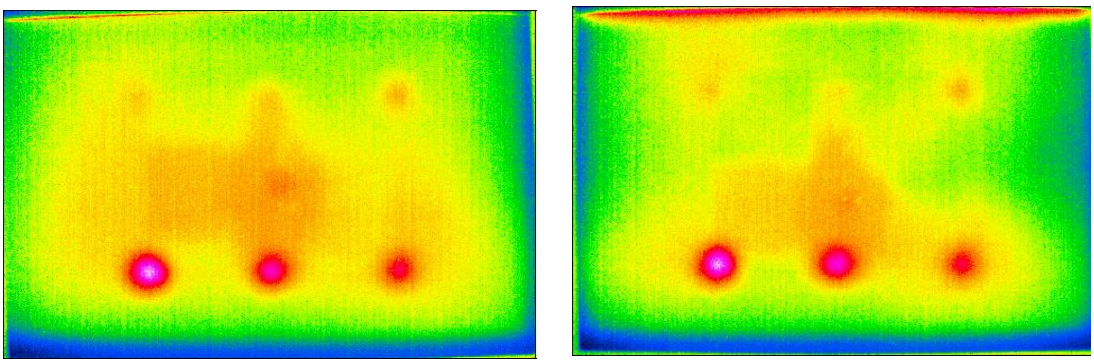

30 cm 35 cm

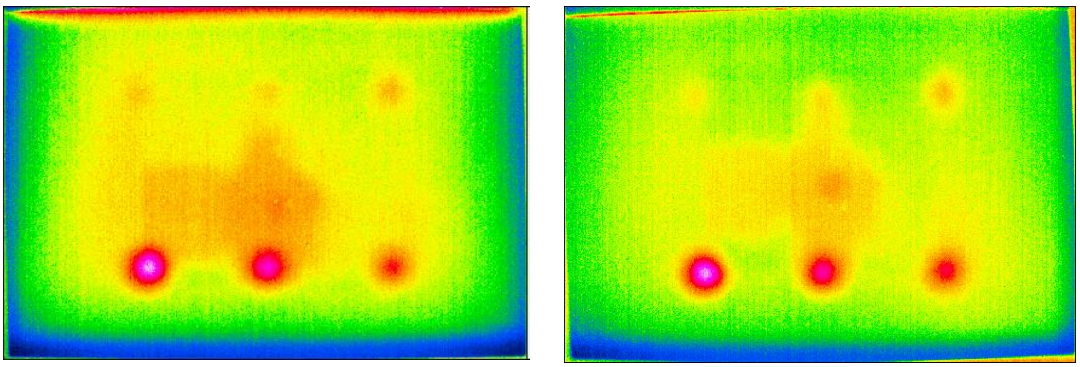

40 cm 45 cm

Fig. 3.9. Comparison of different distances.

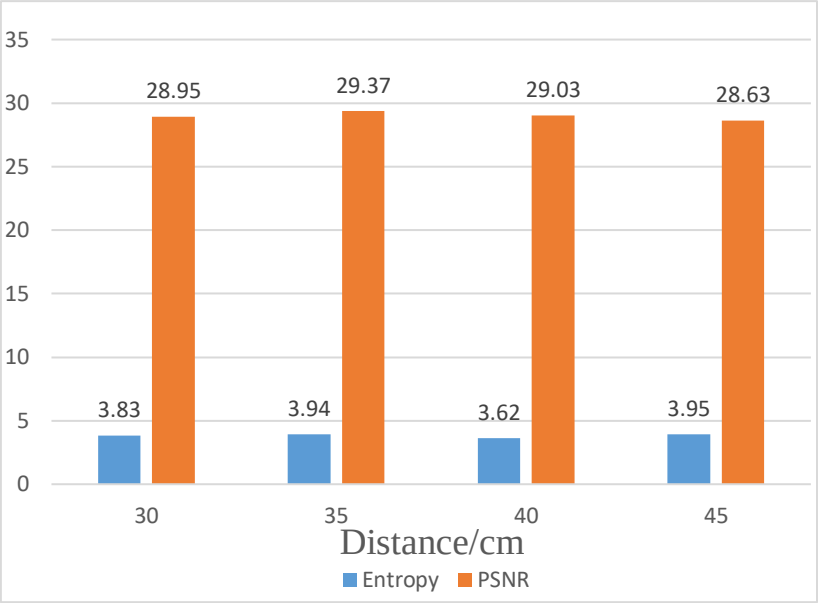

Fig. 3.10. Peak SNR Results.

3.4 Design and Construction of Super-Resolution Neural Network

3.4.1 Generator Design

In the initial generation model of SRGAN, a residual module is used. This structure uses two convolutional layers, two BN layers, and a PReLU function. The schematic diagram of the residual module structure is shown in fig. 3.11.

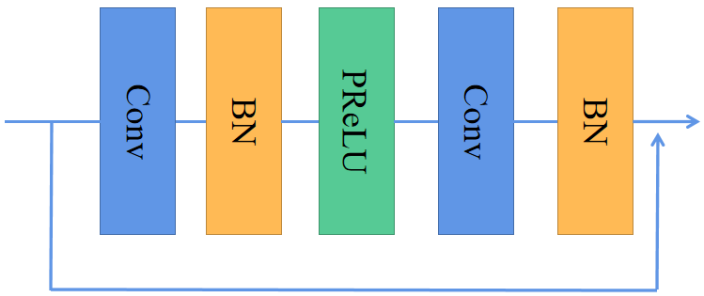

Fig. 3.11. Schematic diagram of the residual block structure of the SRGAN generator.

In ESRGAN[64], it is proved that the use of BN layers in super-resolution affects the experimental results, considering that removing the BN layers can reduce the

computational complexity while enhancing the expressiveness of the network. The main function of the BN layer is to normalize the variance and mean of each batch of features in the training data set, which leads to artifacts if the features of the training set and test set are different, destroying the effect of super-resolution.

Therefore, it is necessary to improve the generator. According to the theory of ESRGAN, the BN layer in the residual structure of the original generator is removed, and a dense residual block (RRDB)[64] is introduced at the same time. This structure is compared with the residual block. (RB) combines multi-level residual networks and dense connections to prevent the loss of part of the image information during forward and reverse transmission, so that the network depth is increased and the model performance is enhanced. The existing research conclusions show that the deeper the network, the more A good receptive field means that more information in the image can be used, and finally a super-resolution image with excellent effect can be generated. A schematic diagram of the result of the dense residual block is shown in fig. 3.12.

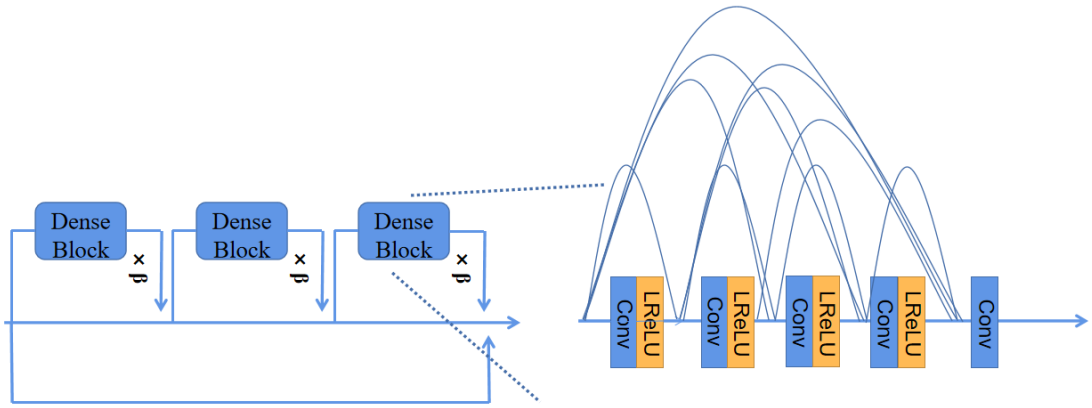

Fig. 3.12. Schematic diagram of dense residual block structure.

3.4.2 Loss function

In the choice of the loss function, choose traditional loss functions: adversarial loss function, content loss function, and TV loss function, and use these functions to train the model.

The adversarial loss function is mainly used in supervised learning. Its main function is to make discriminator D unable to discriminate the distribution of the data. The discriminator D has the same loss condition for all fake data, that is, the output result of the real image is determined. 1, otherwise a fake image outputs 0 as the result.

$$l_{Gen}^{SR} = \sum_{n=1}^{N} -\log D_{\theta_D}\left(G_{\theta_G}(I^{LR})\right) \tag{3.2}$$

The purpose of using MSE as the loss function in the traditional super-resolution network is to make the generated super-resolution image have a higher PSNR, but although this approach can generate images with a higher PSNR, it is effective in detail features. Not good, so this article uses the content loss function, its main function is to pass the super-resolution image generated by the generator G to the VGG16 network for feature extraction, and then use the mean square error on this basis.

$$l_{VGG/i.j}^{SR} = \frac{1}{W_{i,j}H_{i,j}}\sum_{x=1}^{W_{i,j}}\sum_{y=1}^{H_{i,j}}\left(\phi_{i,j}(I^{HR})_{x,y} - \phi_{i,j}\left(G_{\theta_G}(I^{LR})\right)_{x,y}\right)^2 \tag{3.3}$$

The network model will also use the TV loss function, which is a regularization loss function, in order to make the generated super-resolution images smoother and reduce pixel noise.

$$l_{TV}^{SR} = \frac{1}{r^2WH}\sum_{x=1}^{rW}\sum_{y=1}^{rH}\left\|\nabla G_{\theta_G}(I^{LR})_{x,y}\right\| \tag{3.4}$$

3.5 Super-resolution experiments

To ensure that the data obtained in the experiment is not affected by the equipment configuration, the equipment used in the experiment will remain the same. table 3.1 shows the computer configuration and compilation environment used in the laboratory.

When training the network, the training data set is divided into different batches. Each batch specifies a specific number of images. During training, the size of each

batch is set to 32, and a total of 100 Epochs are trained. The network optimization model uses the commonly used Adam.

Table 3.1

Experimental configuration

Experimental configuration	
Operating system	Windows11
CPU	Intel Xeon Platinum 8124m @3.0GHz
GPU	NVIDIA RTX 2080Ti ×2
Programming language	Python
Deep learning framework	Pytorch

The FLIR dataset is used as the training set and test level. The dataset contains 2648 images, including infrared images and visible light images, 400 images are used as the validation set and 100 images are used as the test set.

3.6 Experimental results

The trained super-resolution network model was put into the experiment, and the nearest neighbor interpolation algorithm and bicubic interpolation algorithm were used for comparison experiments. The commonly used Urban100, BSD100, Set5, and Set14 data sets were compared. The results are as follows:

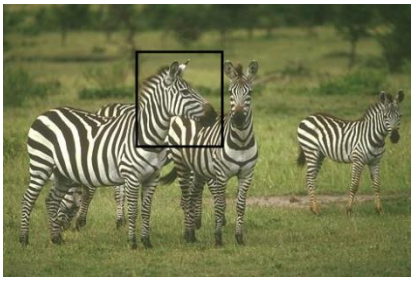

(a) Origin graphic

Origin

Nearest

Bicubic

OURS

(b) Origin graphic

Origin

Nearest

Bicubic

OURS

Fig. 3.13. Partial results of the BSD dataset.

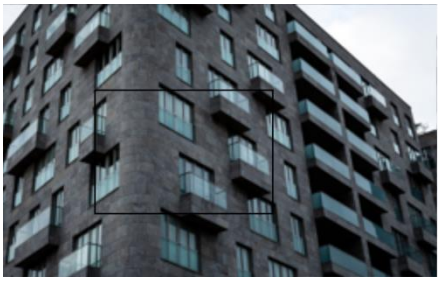

(a) Origin Graphic

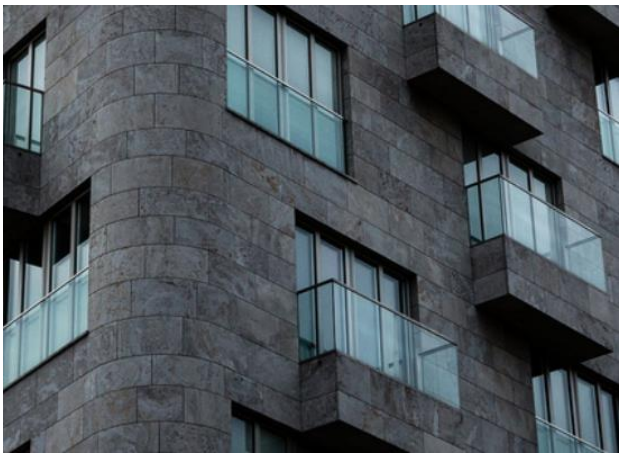

Origin

Nearest

Bicubic

OURS

(b) Origin graphic

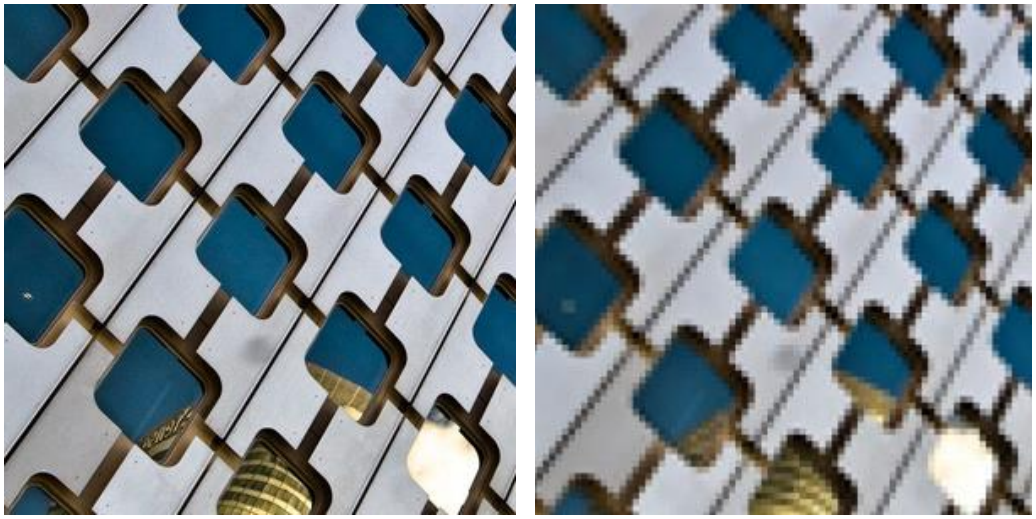

Origin Nearest

Bicubic OURS

Fig. 3.14. Partial results of the Urban dataset.

(a)Origin graphic

Origin

Nearest

Bicubic

OURS

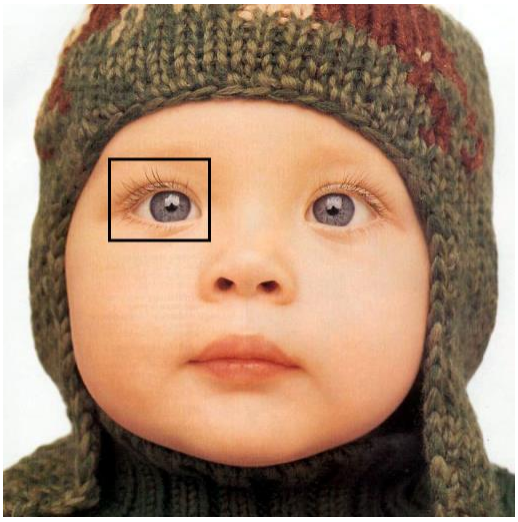

(b) Origin graphic

Origin Nearest

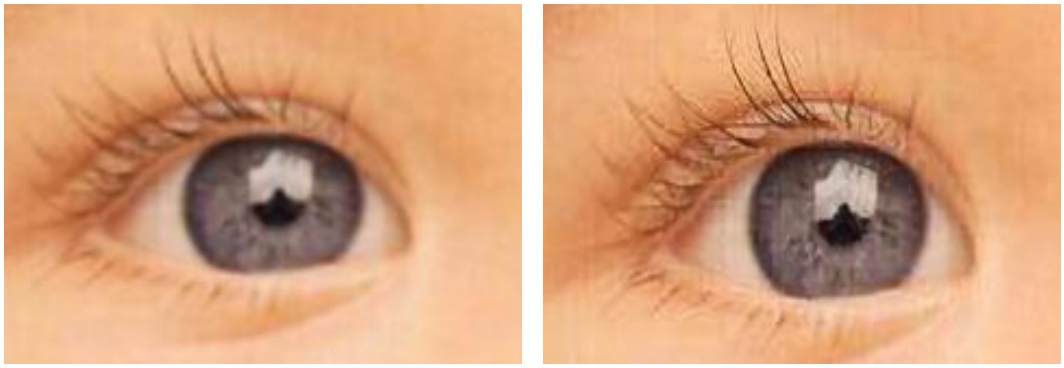

Bicubic OURS

Fig. 3.15. Partial results of the Set 5 dataset.

According to the experimental results, it can be seen that the nearest neighbor interpolation effect is the worst, the bicubic interpolation effect is second, and the super-resolution image generated by our GAN-based algorithm is the best.

Calculate the PSNR and SSIM for each data set separately, and get the results, as shown in Table 3.2.

Table 3.2

Model	Set 5	Set 14	BSD 100	Urban 100
	PSNR/SSIM/MOS	PSNR/SSIM/MOS	PSNR/SSIM/MOS	PSNR/SSIM/MOS
Bicubic	28.37/0.8196/2.03	25.13/0.7329/1.95	25.83/0.7491/1.47	24.71/0.732/1.934
Nearest	26.37/0.7476/1.76	24.63/0.7133/1.23	25.19/0.6542/1.54	23.42/0.6132/1.31
OURS	29.743/0.874/3.89	26.476/0.771/3.64	24.98/0.6429/3.11	25.176/0.7361/3.57

According to PSNR, SSIM, and MOS data, it can be seen that our super-resolution algorithm is better than the traditional interpolation algorithm in objective results in most cases. In the BSD100 dataset, the PSNR data is slightly lower than the traditional interpolation algorithm, but the MOS value is undoubtedly far superior to other algorithms. It can be concluded that our algorithm is much better than other algorithms in the visual sense of the human eye, and the generated images are more detailed.

3.7 Infrared Nondestructive Testing Super Resolution Experiment

Perform super-resolution experiments on the infrared detection images obtained in the previous experiments, and the results are shown in fig. 3.16.

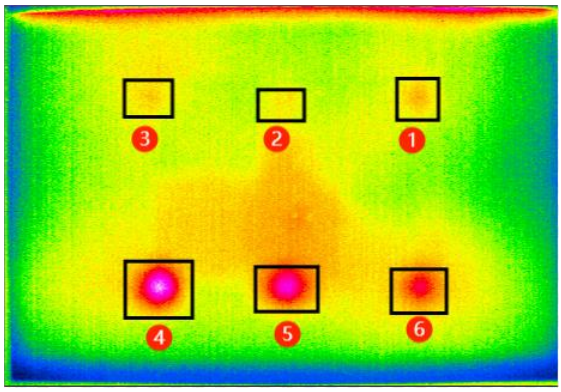

(a) Experimental result

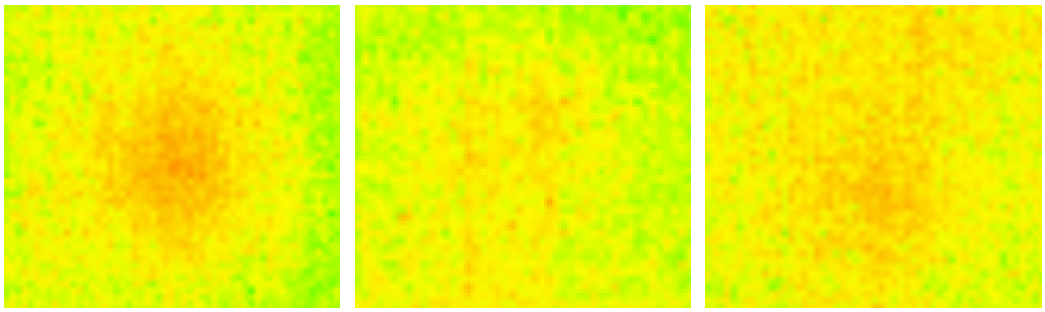

1 2 3

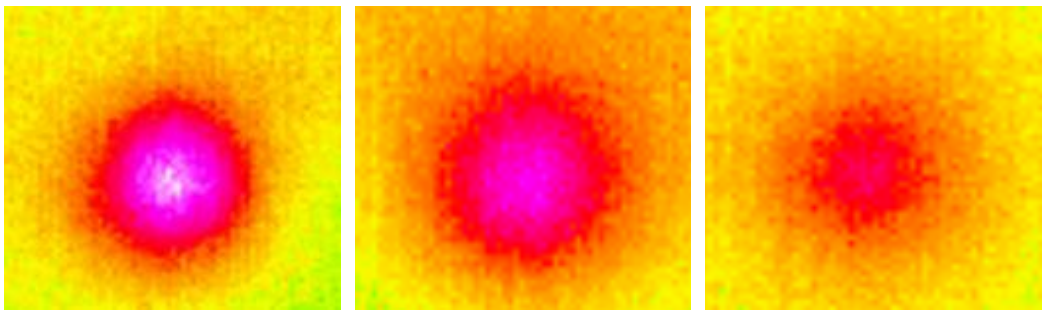

4 5 6

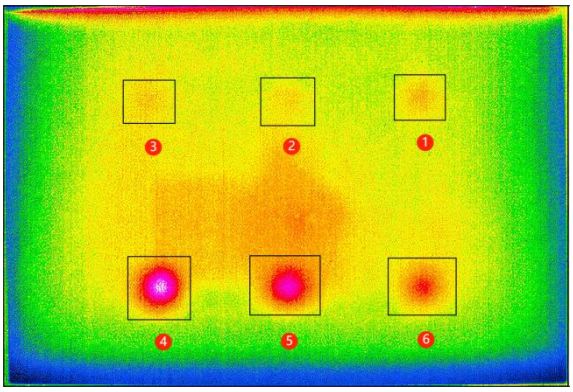

(b) Super-resolution result

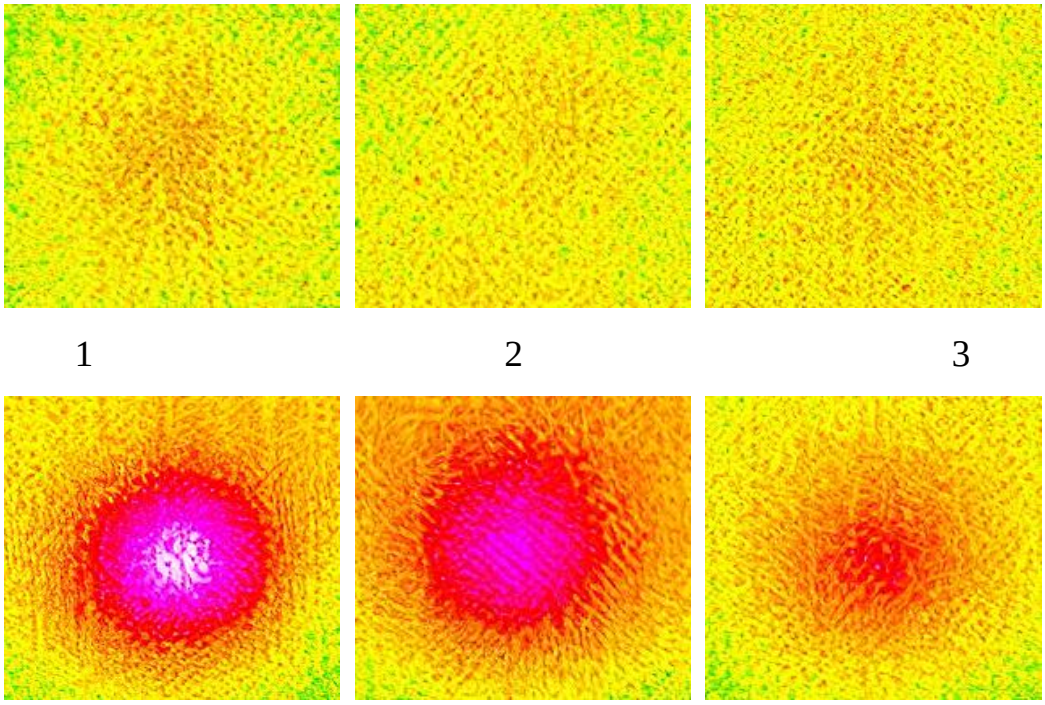

1 2 3

4 5 6

Fig. 3.16. Super-resolution results.

It can be seen from the super-resolution experimental results that our algorithm can also perform super-resolution processing on infrared detection images, and after super-resolution, it has better contrast, image clarity, and edge contours become clearer, which can make The defect detection effect better, laying a good foundation for the future defect identification and detection.

Conclusion for part 3:

By constructing a super-resolution model and performing super-resolution experiments on images, the feasibility of the method is verified. Not only super-resolution experiments are carried out on infrared non-destructive testing images, but also super-resolution reconstructions carried out on complex images in the natural environment. Through the objective evaluation data PSNR and SSIM, as well as the subjective evaluation data MOS, it can be concluded that the super-resolution algorithm based on the generative adversarial network has better performance than the traditional interpolation algorithm, which is suitable for the future automatic nondestructive detection, intelligent defect detection Identification, and online non-destructive testing have laid a good foundation.

PART 4. LABOUR PROTECTION

Glass fiber is an inorganic non-metallic composite material with excellent performance. It has various applications and is widely used in many industries. It has good insulation properties, heat resistance, corrosion resistance, high mechanical strength, lightweight, etc. characteristics. There are many hidden risk factors in the production process of glass fiber. The occupational disease hazard risk of glass fiber production enterprises is severe. To protect the health of workers and prevent the occurrence of occupational diseases, this chapter will focus on glass fiber manufacturing and conducts a hazard analysis [65].

4.1 Main production process and hazard factors

Glass fiber manufacturing adopts a combination of automation, mechanization, and manual operation. The main process flow is batching → kiln → fiber forming and cotton collection → curing and trimming → veneer → cutting → packaging. Specifically: first, the batch workers pour the crushed broken glass and borax into the mixer for automatic mixing, and then automatically transport them to the kiln by the pipeline, where they are melted into the molten glass at a high temperature of 1300 °C; the molten glass enters the fiber-forming cotton production line is centrifuged into fine glass fibers, and at the same time, the adhesive is sprayed to make the glass fibers gather into tires, and then automatically sent to the curing furnace for curing (curing temperature 200 ℃), and the cured glass wool is directly and automatically trimmed; The veneer uses the hot melt adhesive heated to 100 ℃ to automatically veneer the veneer material and the glass wool after trimming on the veneer, and after cutting by the cutter, it becomes a glass wool product of various specifications.

4.2 Harmful factors in glass fiber manufacturing

Skin allergies: the most common hazard in the glass manufacturing industry is skin irritation and allergy. After investigation, 70% of employees who have been exposed to glass fiber for less than a week will have skin allergies of varying degrees, which often occur on the back of the hand, between the fingers, and on the arms. , on the face and other parts, the common phenomenon is needle-shaped erythema, which is unbearable itching. Most employees use anti-allergic drug treatment, and the symptoms will disappear in a few days, while a small number of employees may have more serious symptoms, such as edema, suppuration, high fever, and other symptoms, if such a situation occurs, the employees must stop contacting glass fiber and cooperate with medical treatment. Generally, the symptoms will disappear after treatment, and the main cause of skin allergy is related to glass fiber processing that is related to chemicals.

Dust and harmful poisons: the crushing, batching, and transportation of raw materials for glass fiber production will generate a lot of dust, and many toxic substances will also be generated in the production work, such as glass wool dust, broken glass dust, borax dust, ammonia, phenol, etc. Glass dust is mainly produced in the process of glass fiber spinning. It floats in the air of the workshop for a long time. When this dust falls on the skin or clothes, it becomes a puncture-like shape, which is difficult to find and falls off. Penetration into the superficial layers of the skin can cause bacterial infection and lichen-like secondary damage to the skin. At present, most of the sizing agents used by glass fiber manufacturers in my country are purchased products. In order to keep the information of the products confidential, the sizing enterprises will not indicate the ingredients and usage matters. It was found to have an irritating odor and cause allergy and corrosion to the skin. After air composition testing, it was found that there are harmful gases such as benzene, toluene, xylene, benzene series, carbon monoxide, and ammonia.

Heat radiation: glass fiber production requires melting furnaces, which generate a lot of thermal radiation and glare, which can cause damage to human skin and eyes.

Noise: motors in workshops that shred material, blowers at the bottom of melting furnaces, and textile workshops generate a lot of noise that can cause damage to a person's hearing system[66].

Table 4.1

Distribution of hazard factors

Process	Type of work	work location	Hazardous factors
Ingredients	Batching worker	Dosing operation position	Other dusts (broken glass dust, borax powder dust), noise
Kiln	Kiln worker	Kiln inspection position	Silica dust, high temperature
Fiber collection	Fiberizer	Centrifugal fiber-forming inspection station	Silica dust, phenol, formaldehyde, ammonia, noise, high temperature
Cured trim	Curing worker	Curing and trimming inspection position	Glass wool dust, phenol, formaldehyde, ammonia, noise, high temperature
Veneer	Veneer	Veneer operating position	Glass wool dust, high temperature
Cutting	Cutter	cutting operation position	Glass wool dust, noise
Package	Packing worker	Wrapping bits	Glass wool dust, noise

Table 4.2

Dust detection results of a glass fiber manufacturing plant

Dust					
Glass wool dust (total concentration time-weighted average allowable concentration PC-TWA 3mg/m³, the maximum overrun multiple is 2)					
Position/Type of Work	Detection value/(mg/m³)	Contact time/(h/d)	Test results		
			Time-weighted average allowable concentration/(mg/m³)	Over-limit multiple	Conclusion
Loader	3.4～3.86	1.2	0.52～0.55	＜2	Qualified
wire drawing worker	0.5～0.72	12	0.91～1.05	＜2	Qualified
Spinner 1	0.5～0.76	12	0.86～0.94	＜2	Qualified
Spinner 2	0.6～0.83	12	1.01～1.13	＜2	Qualified

Table 4.3

Chemical test results of a glass fiber manufacturing plant

Formaldehyde (occupational exposure maximum allowable concentration MAC 0.5mg/m³)					
Position/Type of Work	Detection value/(mg/m³)	Contact time/(h/d)	Test result MAC/(mg/m³)	Conclusion	Job Grading
Loader	0.28-0.31	1.2	0.29-0.31	合格	0

Table 4.4

Test results of physical factors in a glass fiber manufacturing plant

Noise (occupational exposure limit: L_{EX40h}85dB(A))					
Position/Type of Work	Detection value dB (A)	Contact time/(h/w)	Test results		Job Grading
			Equivalent sound levelL_{EX40}dB（A）	Conclusion	
Loader	85.6～86.4	1.2	77.5～78.3	Qualified	/
wire drawing worker	88.5～89.4	12	90.7～91.3	Failed	2
Spinner 1	91.4～92.5	12	93.5～93.8	Failed	2
Spinner 2	91.6～92.6	12	93.5～93.7	Failed	2

Analysis of the test results: The four positions in the glass fiber production plant that may have glass dust were tested [67], and the results were all in line with the occupational exposure tolerance.

The positions of the glass fiber factory where formaldehyde poisonous gas may be present were tested [68], and the test results met the occupational exposure tolerance and reached the action level.

Four potentially noisy positions in the glass fiber factory were tested [69]. The results showed that the noise of the feeding positions did not exceed the occupational exposure tolerance and did not reach the action level; the remaining 3 positions exceeded the occupational exposure tolerance and were classified as level 2. Noise work.

4.3 Analysis of working conditions and formulation of protective measures

Ways to prevent skin allergies: it is required that when entering the workshop, staff must wear rubber gloves, apply skin care cream, change work clothes on and off work, cannot enter and leave the workplace at will, and clean after work. Work clothes cannot be put together with other clothes, and must be placed in a dedicated place. It is strictly forbidden to bring work clothes home to avoid skin allergies for non-staff members. Use high-temperature water to clean work clothes to prevent glass fiber and other dust from adhering to work clothes for a long time. Inflict secondary damage. Carry out skin protection safety knowledge training for staff, improve staff's awareness and understanding of this aspect, and use the theoretical knowledge learned in practical work.

Dust and toxic substances protection methods: in the production workshop, especially the crushing and batching workshops, sufficient and effective dust collection and air purification equipment must be installed. When designing the geographical location of these special workshops, they should be as far away from other production workshops as possible, and the transportation of raw materials for glass fiber production must be closed. It can prevent the harmful substances in the raw materials from drifting into the air for diffusion, which will cause harm to the health of surrounding people. Strengthen the air circulation in the textile workshop, and the staff must wear dust masks, safety helmets, and tight-fitting work clothes to prevent poisonous substances from passing through the clothes and irritating the skin.

Thermal radiation protection method: The melting furnace used in the glass fiber production plant will generate a large amount of thermal radiation, which may cause damage to the exposed skin of the staff. Therefore, the staff must be required to wear protective clothing and protective masks to protect their bodies. To carry out the necessary protection, it is also necessary to require that workers should not stay around the melting furnace for a long time, stay away from the melting furnace as far as

possible, and use heat-absorbing glass to isolate the melting furnace from other workplaces. And the melting furnace is an automatic operation, and a small number of workers can be arranged for an inspection.

Noise protection: The crushing workshop of the glass fiber production plant, the blower at the bottom of the melting furnace, and the textile workshop are the main sources of noise. The noise-producing equipment must be controlled, and the hearing protection of the staff must be strengthened, such as setting vibration damping pads for the noise-generating equipment, etc. Noise-canceling facilities, distribution of earplugs to staff to protect hearing systems, etc. When designing the workshop layout, it should be considered that other workplaces should keep a certain distance from these noise-producing workshops to reduce the impact of noise on other workers[70].

4.4 Fire safety in the workplace

There are flammable and explosive harmful gases in the workshop of the glass fiber manufacturing plant, which may lead to the occurrence of fire. The air circulation device in the workshop should be strengthened to reduce the concentration of flammable, explosive, and toxic gases in the workshop, and the concentration of such harmful gases should be installed. Monitor the sensor, check the gas concentration regularly, adjust the working status of the workshop in time, and prevent the occurrence of fire.

Part of the dust existing in the workshop may also be easily combustible, and may also have conductive properties. If there is an exposed circuit without a protective cover in the workshop, it is extremely easy to cause a short circuit of the circuit, resulting in a fire. This kind of non-existent circuit should be avoided in the workshop. Protected circuit devices, if possible, should be installed in places that do not have these safety hazards and are easy to maintain.

In the overall use of materials in the workshop, the structure of fire-proof materials should be installed. Once a fire occurs, it will not immediately endanger the staff working in the workshop, increase the escape time, and install fire-fighting equipment in conspicuous places in the workshop, such as various The number of fire extinguishers, gas masks, water pumps used for firefighting, etc., will minimize the fire hazards in the factory.

PART 5. ENVIRONMENTAL PROTECTION

Glass fiber is an inorganic non-metallic material with excellent performance. It is made of natural inorganic non-metallic minerals such as pyrophyllite, quartz sand, and limestone as raw materials, and is processed by several processes such as high-temperature melting, wire drawing, and winding according to a certain formula. , It has the advantages of being light-weight, high strength, high-temperature resistance, corrosion resistance, heat insulation, sound absorption, and good electrical insulation performance. Glass fiber can replace steel, aluminum, wood, cement, PVC, and other traditional materials, and is widely used in transportation, construction and infrastructure construction, electrical and electronic, environmental protection and other industries.

With the increase of environmental protection and safety supervision, the production and application of downstream composite products tend to be standardized, the demand for clay and crucible ball drawing products has been greatly reduced, and the demand for alkali-free and high-performance glass fibers has steadily increased. At the same time, the market demand for thermoplastic yarn, electronic yarn, and other products continued to maintain rapid growth, and the supply and demand in some markets became tighter. Reinforced plastic with glass fiber or its products as reinforcement material is called glass fiber reinforced plastic, or glass fiber reinforced plastic. At present, most FRP products in our country are made of thermosetting resins, which are not easy to degrade, decompose and recycle.

The traditional burial and incineration methods occupy a lot of lands, cause environmental pollution, the treatment cost is high and the treatment capacity is limited, which is far from meeting the requirements of the sharp increase in the amount of FRP waste. With the increasingly strong environmental protection calls for FRP waste recycling, FRP waste has become a social problem, which seriously affects the further

application of FRP in building materials, automobiles, and other industries. In addition, FRP waste cannot be reshaped by heating like thermoplastic FRP (FRTP), and it is often painted, painted, and used in conjunction with other plastic parts during use, which makes it difficult to recycle. In addition, on October 27, 2017, the World Health Organization's International Agency for Research on Cancer published a preliminary list of carcinogens for reference. Fibers for special purposes, such as E glass and 475 glass fibers, are listed in the list of 2B carcinogens, and continuous glass fibers are listed in the list of 3 carcinogens.

An important growth area for FRP is the preparation of wind turbine blades and towers for wind power generation. On February 14, 2018, the Global Wind Energy Council released the annual statistical report on the global wind power market, stating that the global market added 52.57 GW of installed capacity in 2017, and the cumulative installed capacity reached 539.58GW. Among them, Europe, India, and offshore wind power installations achieved record breakthroughs. The growth rate of wind power in China has slowed down, with 19.5 GW of installed capacity, still accounting for more than 37% of the world's new capacity that year. 10 kg of blade material is expected to be required for every 1 kW of newly installed capacity, so a 7.5 MW wind turbine would require approximately 75 tonnes of blade material. With the increase in wind turbine capacity, the length of the blade increases, and the amount of carbon fiber also increases: for example, the length of the 6MW wind turbine blade is 75 meters, and the length of the 12MW wind turbine blade reaches 107 meters, and a single piece weighs 50 tons. Wind turbine blades currently produced are made of glass fiber (GF), carbon fiber (CF) or glass fiber/carbon fiber composite reinforced thermosetting resin matrix composites, which are widely used. However, composites are difficult to recycle because their matrix is a cross-linked thermoset polymer that cannot be remelted or reshaped. This is based on the inherent heterogeneity of thermoset polymer composites. Several recent studies have shown that the use of

carbon fiber reinforcements in the load beam portion of the blade does hold promise for cost-effective weight savings and stiffness gains. In particular, the emergence of new low-cost large tow carbon fibers can provide blades with lower cost and better structural performance compared to all-glass fiber reinforced blades. If carbon fiber can meet both structural performance requirements and sufficient production efficiency, it will be more economical to use carbon fiber. Stitched hybrid fabrics and other automated performing processes hold great promise in the blade manufacturing industry. Maintaining fiber straightness is an important factor in obtaining optimal compressive strength from composite materials. Carbon fiber, its stiffness, and tensile strength are relatively good, and in order to obtain all of these excellent properties, it is required to make fabric/preformed structures, and these forms of products are also beneficial to obtain good compressive strength.

5.1 Research progress of FRP waste recycling at home and abroad

European and American countries and Japan and other countries have widely reported on the recycling of waste FRP. There are also articles in the FRP publications in my country. The following is an introduction to the scientific research progress on recycling in the UK for reference. The recycling of FRP waste in the UK is included in the Plastics Recycling Project, led by the British Plastics Federation, under which there is a Thermoset Plastics Committee, and so far, 20 companies have participated, including FRP processing plants and resins, fillers and glass. Fiber Manufacturing Plant. A research project in the UK's Bruno University laboratory will provide information and seek new methods of recycling thermoset plastics. At the school's Wolfson Materials Processing Center, research began on the use of recycled thermoset plastic fragments, which include polyester, phenolic, amine-based, and epoxy-based plastics. These FRP scraps were ground and used as fillers in the processing of thermoplastics such as polypropylene and FRP. Another project, which took waste FRP

as an energy recovery project at the University of Nottingham, used FRP mainly from automotive SMC (SMC composite material is the abbreviation of the Sheet molding compound, that is, sheet molding compound). Energy recovery is attractive. Tests have shown that FRP made of unsaturated polyester, epoxy, and phenolic resin can generate heat energy when burned, and does not produce harmful polluting gases.

Table 5.1

Comparison of recycling methods

Type	Methods	Scope of application	Recycled product	Application
Chemical recycling	Pyrolysis	Including contaminated waste	Pyrolysis gas, pyrolysis oil, solid by-products	Used as fuel, Thermoplastic, etc.
Physical recycling	Smash	Only for uncontaminated waste	Powder	Plastics, Coatings, etc.
Energy recovery	Incinerate	Only suitable for waste with high resin content	Heat	Power generation, Heat source

5.2. Glass Fiber Recycling Methods

Pyrolysis method: The American Automobile Association and General Motors worked together, and in 1988 and 1989, Conrad Industries and Wind Gap, J. H. Beers carried out tens of tons of SMC waste pyrolysis experiments, which confirmed the feasibility of the pyrolysis method. sex. The pyrolysis method is to learn from the high-temperature decomposition and recovery method of plastics and rubber, and heat and decompose the glass fiber-reinforced plastic waste into pyrolysis gas and pyrolysis oil that preserves energy components, as well as solid by-products mainly CaCO3 and glass fiber in the absence of oxygen. The pyrolysis products vary with the pyrolysis

temperature. Generally, the pyrolysis oil is mainly recovered at 400℃-500℃, and the pyrolysis gas is mainly recovered at 600℃-700℃. Once the pyrolysis process starts, i.e. the temperature reaches 480℃-980℃, the generated pyrolysis gas has enough energy for pyrolysis to be self-sufficient, and the excess part can be stored as fuel. The pyrolysis process and final product meet safety and environmental requirements. The biggest advantage of pyrolysis is that it can process FRP waste contaminated with paints, adhesives, and other materials, while the metallic foreign matter is removed from the solid by-products after pyrolysis. Pyrolysis is the most promising recycling technology.

Mechanical (pulverizing) recycling method: If the FRP waste is not polluted, the mechanical (pulverizing) recycling method is the best recycling method. The recycled pellets and powders can be applied to SMC and BMC like CaCO3, depending on the application. For particle size and size range, see Table 4. FRP waste recycling coarsely pulverized pellets are used for BMC, and the dosage can reach 50%; the powder is used for the powder to replace CaCO2 filler and glass fiber. The performance is improved by 50-100%. Density drops by 10-15%. The crushing and recycling method is the most preferable in terms of technical feasibility and practicality. There are many types of recyclable thermosetting composite wastes, and the thermosetting composite wastes (such as SMC waste) that are difficult to be recycled by general methods can also be recycled well without causing pollution to the environment, which is a solution to thermosetting composite materials. An important development direction of waste pollution.

Mechanical recycling methods: Many recycling techniques for thermoset composites have been proposed and developed, and there are basically two types of processes: one involves mechanical shredding techniques to reduce the scope of waste and produce recyclable products; the other uses thermal processes Recycling waste into materials and heat[71].

.Glass fiber waste is one of the wastes generated in the production process of glass fiber. It is a kind of solid waste, and countries around the world are gradually increasing their efforts to protect the environment. Otherwise, it will bring harm to the glass fiber manufacturing industry, society, people's life, and many other aspects. The treatment of glass fiber waste has always troubled production enterprises. In the past when environmental protection was not strong, the waste was treated by deep burial, but it caused a lot of land pollution. It is no longer advisable, so we must find a more suitable way to solve the problem of environmental pollution.

5.3 Glass fiber waste recycling method

Waste silk crushing and impurity removal First, the long waste silk is crushed into short waste silk with a length of about 10-20mm in the crusher. During the crushing process, water is added to rinse it at the same time to remove a part of the infiltrating agent attached to it, and then stored, Naturally drain the water to a moisture content of about 5%, pass the glass fiber waste wire through the vibrating screen to remove large impurities, temporarily stored in the silo, and then add the waste wire evenly and stably to the belt conveyor, which is equipped with an electromagnetic iron remover. , remove iron impurities, enter the elevator, and prepare to be sent to the incinerator for incineration. Since the final product of this process needs to be recycled as a glass fiber raw material, the quality of the glass fiber raw material must not only meet the requirements of the established components, but also ensure that the content of impurities and associated minerals is low, the content of iron is low, and the content of chromium is as low as possible. Raw materials of refractory heavy minerals such as iron ore and chrome spinel[72]. Therefore, it is necessary to configure impurity and iron removal process equipment in this process. What needs to be discussed here is the necessity of electromagnetic iron remover. Because in the production process of glass fiber, some metal impurities will be mixed into the waste wire during the replacement

of the leakage plate in the forming process and the equipment maintenance process, such as bolts, nuts, welding rods, and cutting blades, etc. These impurities can be removed as much as possible. It greatly reduces the damage to the grinding equipment during the grinding process, and at the same time reduces the pollution to the final product. There are many ways to remove iron impurities. The scheme used in this process is to evenly spread the crushed short waste wire on the belt conveyor, and then install an electromagnetic iron remover on the upper end of the belt conveyor to remove iron impurities.

A large amount of organic sizing agent is used in the production process of glass fiber waste incineration, so there will also be a large amount of organic sizing agent on the surface of glass fiber waste filament. Although it has been washed with water during the crushing process, there is still a large part of it attached to the waste glass fiber. If these organic substances are directly brought into the kiln for melting, it will affect the redox atmosphere in the kiln, thereby affecting the melting quality of the molten glass, which is very unfavorable for normal wire drawing operations[73]. Therefore, a special incinerator is needed to completely incinerate these organic sizing agents, and only the inorganic glass waste filaments are retained, so as to ensure that the recycled waste filaments are as clean as possible. Etc.: The discussion of the glass fiber waste recycling process and application technology research and use requirements can achieve better use results. The waste wire enters the feeder of the incinerator, and after being incinerated at high temperature, the organic sizing agent attached to the surface of the glass fiber waste wire is completely removed, and then automatically unloaded, cooled, and transported by a conveyor with a cooling device, and finally Into a transition silo for cooling and storage, ready for grinding. Temperature control during incineration is also more critical. It is necessary to set different incineration temperatures according to different sizing agents, so as not to waste energy during the incineration process as much as possible.

The waste silk after grinding and sieving and burning enters a transition silo, and then is uniformly and stably added to the ceramic ball mill for grinding according to the set requirements. The finished product is under the sieve, which is automatically packed in tons of bags. The coarse particles on the sieve enter another vibrating screen. The coarse material under the sieve enters the ball mill again through the return conveyor for grinding. The large particles on the sieve are some impurities, including Impurities such as some sawdust, stainless steel or iron bolts, and nuts that have not been removed. In this process, the impurities in the glass fiber waste are removed again, so as to reduce the impurity content in the glass fiber waste as much as possible. In this process, the selection of the grinding host is the key. There are many kinds of grinding equipment, such as iron ball mills, ceramic ball mills, Raymond mills, etc. The main reason for choosing a ceramic ball mill for this process is that the iron ball mill, Raymond mill, etc., in the process of grinding glass fiber waste wire, due to the high hardness of the glass, the iron grinding medium of the mill is worn very seriously. The important thing is that the worn iron impurities enter the finished product together with the glass fiber waste wire powder. The iron impurities can easily lead to the scrapping of the subsequent drawing bushing due to iron poisoning[74], so its existence has a serious impact. to the quality and effect of recycling. The use of a ceramic ball mill can completely avoid this unfavorable situation. Its grinding mechanism is more suitable for the grinding of this hard glass waste wire. The main reason is that the ceramic ball mill uses ceramic lining (high aluminum) and ceramic balls (high Aluminum) as the grinding body, the contact with the glass fiber waste is all ceramic materials, and the main chemical composition of the ceramic material is Al2O3, which is also part of the chemical composition of the glass fiber, so the use of a ceramic ball mill will not cause any raw material pollution[75-78].

In the whole process system, during the process of unloading, incinerating, grinding, and sifting glass fiber waste, it will inevitably generate a lot of dust. The main

component of this dust is glass fiber particles, which are very harmful to operators[79], so it is necessary to carry out centralized dust collection treatment on these dust points, which is conducive to environmental protection and maintenance of workers' occupational health. The main way of dust collection is to use a high-temperature resistant cloth bag dust collector, through the ventilation of the exhaust fan, so that each dust point is in a negative pressure state, once there is dust leakage, it is immediately evacuated by the exhaust fan, and then collected through the cloth bag[80].

Conclusion:

Glass fiber is a non-metallic composite material with excellent performance, but the by-products generated after its production are still a problem that cannot be ignored. There are still some shortcomings in various recycling technologies, but the situation is compared with the past. A very large improvement, the degree of pollution to the environment is reduced with the development of recycling and waste treatment technology.

REFERENCES

1. 郑传祥. 复合材料压力容器[M]. 化学工业出版社, 2006.1-2

2. 张道海, 何敏, 郭建兵,等. 相容剂对长玻纤增强聚苯乙烯复合材料性能的影响[J]. 高分子学报, 2014(3):378-384.

3. 廖晓玲, 王强, 谷小红,等. 基于 THz-TDS 的碳纤维复合材料无损检测[J]. 激光与红外, 2015, 45(10):1255-1260.

4. 朱延霆. 基于 X 射线数字成像技术的缠绕气瓶检测研究[D]. 北京：北京化工大学,2014.

5. 唐庆菊. SiC 涂层缺陷的脉冲红外热波无损检测关键技术研究[D]. 哈尔滨: 哈尔滨工业大学博士学位论文, 2014: 10-20.

6. 刘颖韬, 郭广平. 红外热像无损检测技术的发展历程、现状和趋势[J]. 无损检测, 2017, 29(8): 63-70.

7. 魏嘉呈, 刘俊岩. 红外热成像无损检测技术研究发展现状[J]. 哈尔滨理工大学学报, 2020, 25(2): 64-72.

8. 周俊宇, 赵艳明. 卷积神经网络在图像分类和目标检测应用综述[J]. 计算机工程与应用, 2017, 53(13): 34-41.

9. Ren S, He K. Faster R-CNN: Towards Real-Time Object Detection with Region Proposal Networks [J]. IEEE Transactions on Pattern Analysis&Machine Intelligence, 2016, 39(6): 1137-1149.

10. Meola C, Carlomagno G. Recent Advances in the Use of Infrared Thermography[J]. Measurement Science and Technology, 2004, 15: 27-58.

11. Almond D, Lau S. Edge effects and a method of defect sizing for transient thermography [J]. Applied Physics Letters, 1993, 62(25): 3369-3371.
12. Vavilov V. Dynamic thermal tomography perspective field of thermal NDT[C]// Proc. SPIE 1313, Thermosense XII: An International Conference on Thermal Sensing and Imaging Diagnostic Applications, 1990, 1313: 178-182.
13. Vavilov V. Dynamic thermal tomography new promise in the IR thermography of solids[C]// Proc. SPIE 1682, Thermosense XIV: An Intl Conf on Thermal Sensing and Imaging Diagnostic Applications, 1992, 1682: 194-206.
14. Melnyk S, Melnyk S, Tuluzov I. Method of projection dynamic thermal tomography (PDTT)[C]// 11th International Conference on Quantitative InfraRed Thermography, 2012: 20-28.
15. Vavilov V, Kuimova M. Dynamic Thermal Tomography of Composites A Comparison of Reference and Reference-Free Approaches [J]. Journal of Nondestructive Evaluation, 2019, 38(2): 1-13.
16. Busse G, Wu D, Karpen W. Thermal wave imaging with phase sensitive modulated thermography[J]. Journal of Applied Physics, 1992, 71(8): 3962-3965.
17. Meola C, Carlomagno G. Non-destructive evaluation of aerospace materials with lock-in thermography[J]. Engineering Failure Analysis, 2005, 13(2006): 380-388.
18. Shrestha R, Choi M, Kim W. Thermographic inspection of water ingress in composite honeycomb sandwich structure: a quantitative comparison among Lock-in thermography algorithms[J]. Quantitative Infrared Thermography Journal, 2019: 1-16.
19. Oliveira B, Nienheysen P. Improved impact damage characterisation in CFRP samples using the fusion of optical lock-in thermography and optical square-pulse shearography images [J]. NDT and E International, 2020, 111: 1-15.
20. Maldague X, Marinetti S. Pulse phase infrared thermography[J]. Journal of Applied Physics, 1996, 79: 2694.

21. Gruber J, Stotter B, Mayr G. Prospects of pulse phase thermography for finding disbonds in CFRP-sandwich parts with aluminum honeycomb cores compared to ultrasonic[J]. American Institute of Physics, 2013: 547-554.

22. Popow V, Martin G. Determination of depth and size of defects in carbon-fiber-reinforced plastic with different methods of pulse thermography [C]// Nondestructive Characterization and Monitoring of Advanced Materials, Aerospace, Civil Infrastructure, and Transportation XII, 2018, 10599: 1-8.

23. Shepard S. Temporal noise reduction, compression and analysis of thermographic image data sequences, US6516084 B2[P]. 2003.

24. Shepard S, Beemer M. Advances in Thermographic Signal Reconstruction [C]// Thermosense: Thermal Infrared Applications XXXVII. International Society for Optics and Photonics, 2015: 30-38.

25. Oswald T, Shepard S. Comparison of pulse phase and thermographic signal reconstruction processing methods [C]// Spie Defense, Security, & Sensing, 2013: 31-39.

26. Roche J, Passilly F, Balageas D. A TSR-Based Quantitative Processing Procedure to Synthesize Thermal D-Scans of Real-Life Damage in Composite Structures [J]. Journal of Nondestructive Evaluation, 2015, 34(4): 40-41.

27. 徐川， 霍雁， 李艳红， 等. 锁相热成像无损检测方法的基础实验研究[J]. 无损检测, 2007, 29(12): 728-730.

28. 姜千辉， 姜长胜， 葛庆平， 等. 红外热波序列图像的图像分割与三维显示[J]. 无损检测, 2008(02): 100-103.

29. 李艳红， 赵跃进， 冯立春， 等. 基于脉冲位相的红外热波无损检测法测量缺陷深度[J]. 光学精密工程, 2008(01): 55-58.

30. 詹绍正， 宁宁， 曲亚林， 等. 红外热成像检测技术在复合材料蜂窝夹芯结构上的应用研究[J]. 结构强度研究, 2009, (4):32-36.

31. Liu J Y, Tang Q J, Wang Y. The study of inspection on SiC coated carbon-carbon composite with subsurface defects by lock-in thermography [J]. Composite Science and Technology, 2012, 72(11): 1240-1250.

32. Liu J Y, Tang Q J, Liu X, et al. Research on the quantitative analysis of subsurface defects for non-destructive testing by lock-in thermography[J]. NDT & E International, 2012, 45(1): 104-110.

33. Liu J Y, Qin L, Tang Q J, et al. Experimental study of inspection on a metal plate with defect using ultrasound lock-in thermographic technique[J]. Infrared Physics & Technology, 2012, 55(4): 284-291.

34. 刘涛， 李永峰， 黄威. BP 神经网络在红外热波无损检测定量识别中的应用[J]. 红外与激光工程, 2012, 41(9): 2304-2310.

35. 周正干， 贺鹏飞， 赵翰学， 等. 钛合金蜂窝结构蒙皮脱焊缺陷锁相红外热成像检测[J]. 北京航空航天大学学报, 2016, 42(9): 1795-1802.

36. 王震， 杨正伟， 陶胜杰， 等. 基于移相技术的含缺陷复合材料锁相热波检测[J]. 红外与激光工程, 2019, S2: 8.

37. Wei J, Wang F, Liu J, et al. A laser arrays scan thermography(LAsST) for the rapid inspection of CFRP composite with subsurface defects [J]. Composite Structures, 2019, 226: 1-8.

38. 陈晓,荆茹韵.单图像超分辨率方法综述[J].电子测量技术,2022,45(09):104-112.DOI:10.19651/j.cnki.emt.2208826.

39. QIN.F, HE X, WU W,et al. Image super-resolution reconstruction based on sub-pixel registration and iterative back projection[M]. Information Computing and Automation, 2008:277-280

40. STARK H, OSKOUI P. Hight-resolution image recovery from image-plane arrays, using convex projections[J]. JOSA A, 1989, 6(11): 1715-1726

41. PATTI A J, ALTUNBASAK Y. Artifact reduction for POCS-based super resolution with edge adaptive regularization and higher-order interpolants [C]. Proceedings 1998 International Conference on Image Processing, 1998: 217-221

42. ELAD M, FEUER A. Super-resolution reconstruction of continuous image sequences[C]. Proceedings of International Conference on Image Processing, 1999,3: 459-463

43. ALAM M S, BOGNAR J G, HARDIE R C, et al. Infrared image registration and hight-reslution reconstruction using multiple translationally shifted aliased video frames [J]. IEEE Transactions on Instrumentation and Mearsurement, 2000, 49 (5): 915-923

44. 陈晓,荆茹韵.单图像超分辨率方法综述[J].电子测量技术,2022,45(09):104-112.DOI:10.19651/j.cnki.emt.2208826.

45. 戴景民,汪子君.红外热成像无损检测技术及其应用现状[J].自动化技术与应用,2007(01):1-7.

46. 李艳玲.图像的最近邻缩放原理及实现[J].长治学院学报,2016,33(05):31-32.

47. Blu T, Thevenaz P, Unser M. Linear interpolation revitalized [J]. IEEE Transactions on Image Processing, 2004, 13(5): 710-719.

48. Lehman T M, G nner C, Spitzer K. Addendum: B-spline interpolation in medical image processing [J]. IEEE Transactions on Medical Imaging, 2001, 20(7): 660-665.

49. Nayak R, Patra D. Image interpolation using adaptive P-spline [C]//Annual IEEE India Conference (INDICON).[S.I.]: IEEE, 2015: 1-6.

50. Zhou D,Shen X, Dong W. Image zooming using directional cubic convolution interpolation [J]. IET Image Processing, 2012, 6(6): 627-634.

51. Hou HS, Andrews H. Cubic splines for image interpolation and digital filtering [J]. IEEE Transaction Acoustics Speech & Signal Processing, 1979, 26(6): 508-517.

52. Keys R. Cubic convolution interpolation for digital image processing [J]. IEEE Transactions on Acoustics Speech & Signal Processing, 1998, 29(6): 1153-1160.

53. Shi J, Reichenbach SE. Image interpolation by two-dimensional parametric cubic convolution[J]. IEEE Transactions on Im-age Processing, 2006, 15(7): 1857-1870.

54. 庞志勇，谭洪舟，陈弟虎.一种改进的低成本自适应双三次插值算法及 VLSI 实现[J].自动化学报，2013，39（4）：407-417.

55. He K, Zhang X, Ren S, et al. Deep residual learning for image recognition[C]. Proceedings of the IEEE conference on computer vision and pattern recognition. 2016: 770-77.

56. Ledig C, Theis L, Huszár F, et al. Photo-realistic images super-resolution using a generative adversatial network [C]. Proceeding of the IEEE Conference on Computer Vision and Pattern Recognition, 2017; IEEE: 4681-4690.

57. Sheikh H R, Bovik AC. Image information and visual quality [J]. IEEE Transaction on Image Processing, 2006, 15(2): 430-444.

58. Liu S, Wu L,Gong Y,et al.Overview of image equality assessment [J]. Science Paper Online, 2011,6(7): 501-506.

59. Sakowicz B, Kaminski M, Ritter R, et al. Methods of 3D images quality assessment [C]//IEEE International Conference on Mixed Design of Integrated Circuits & Systems.[S.I.]: IEEE, 2015: 123-128.

60. Sheikh HR, Sabir MF, Bovika C. A statistical evaluation of recent full reference image quality assessment algorithms [J]. IEEE Transactions on Image pROCESSING, 2006, 15(11): 3440-3451.

61. Wang Z, Li Q. Information content weighting for perceptual image quality assessment [J]. IEEE Transactions on Image Processing, 2011, 20(5): 1185-1198.

62. Wang Z, Gong Y, Sheikh H R, et al. Image quality assessment: From erro visibility to structural similarity [J]. IEEE Transcations on Image Processing, 2014,13(4): 600-612.

63. Schulter S, Leistner C, Bischof H. Fast and accurate image upscaling with super-resolution forests [C]//IEEE International Conference on Computer Vision and Pattern Recognition. [S. I.]: IEEE, 2015: 3791-3799.

64. Wang X, Yu K, Wu S, et al. ESRGAN: Enhanced Super-Resolution Generative Adversarial Networks[C].European Conference on Computer Vision Workshops, Munich, Germany,
2018:63-79.

65. 郭建娜.玻璃纤维生产企业职业病危害状况调查与分析[J].玻璃,2022,49(09):55-58.

66. 朱曙光,郭晓丽.某玻璃纤维生产企业职业病危害现状评价[J].职业卫生与应急救援,2018,36(06):538-540.DOI:10.16369/j.oher.issn.1007-1326.2018.06.022.

67. 郇宜亮.玻璃纤维制造业的职业危害及其预防[J].劳动保护科学技术,1999(02):39-40.

68. GBZ/T192.1~5-2007 工作场所空气中粉尘测定[S].

69. GBZ/T160-2004 工作场所空气有毒物质测定[S]

70. GBZ/T 189.8-2007 工作场所物理因素测量噪声[S]

71. 游敏,肖琴.玻璃钢废弃物机械回收现状研究[J].资源再生,2020(06):52-57.

72. 蔡为仑(Tsai，S．W．)．复合材料设计［M］．刘方龙，王弘生，译．北京:科学出版社，1989．

73. 杨晞明，曾德璋．大学物理学［M］．成都:科技大学出版社，1992.

74. 王继治．玻璃球等材料中亚铁的测定［J］．玻璃纤维，1980 (2):4-6．

75. 张景杰．球磨机与分级机在硅微粉生产线中的应用与配合［J］．有色矿冶，2006(1):121-122．

76. 张壁栋．玻璃配合料［M］．北京:中国建材工业出版社，1992，12:141-142．

77. 黄立．陶瓷球磨机研磨体对筒体作用载荷分析与计算［J］．机械工程师，2006(1):117-119．

78. 李颂华．新型陶瓷球研磨方式的力学分析［J］．沈阳建筑工程学院学报，2002(3):229-232．

79. 房志．防止玻璃纤维粉尘对生产者的危害［J］．职业与健康，1985(4):32-33．

80. 雅楠．浅谈高炉矿槽除尘［J］．化学工程与装备，2010(9):135-136．